THE ASTROPHYSICAL JOURNAL, 343:617–643, 1989 August 15

KINEMATICS OF GAS IN A TRIAXIAL GALAXY

TIM DE ZEEUW
Institute for Advanced Study, Princeton, New Jersey

AND

MARIJN FRANX[1]
Sterrewacht Leiden, Leiden, The Netherlands
Received 1988 September 28; accepted 1989 January 31

ABSTRACT

The morphology and kinematics of cold gas in a triaxial Stäckel potential are discussed. Equilibrium gas disks are allowed in two planes: the plane perpendicular to the long axis and the plane perpendicular to the short axis. General expressions are derived for the projected density distribution and radial velocities. The determination of the aspect angles of the system from observations of the gas and the stellar light is discussed in detail. If a constant M/L is assumed, surface photometry of the stars and the kinematics of one single "ring" of gas suffice to restrict the three-dimensional solution space of the viewing angles to a curve. Observations of two rings in perpendicular planes allow the determination of all three viewing angles, even without the assumption that M/L is constant. If there is an extended gas disk in the plane perpendicular to the long axis, then the complete three-dimensional potential and mass distribution can be determined. Some of the results derived here apply also to gas orbits in nonseparable potentials. If the gas orbit is noncircular, then the geometry of the orbit will cause the locus of zero radial velocity to be different from the apparent minor axis of the gas ring. Such an observation puts direct constraints on the viewing angles and on the flattening of the potential. Further constraints can be found by numerical calculation of the simple periodic orbits in the deprojected potential, and by matching the projected orbit with the measured ring. These results show that allowing for a triaxial shape of the density makes the analysis of the deprojection of gas disks or rings laborious, but is not a major obstacle.

Subject headings: galaxies: internal motions — galaxies: structure — stars: stellar dynamics

I. INTRODUCTION

Bright elliptical galaxies are thought to be triaxial stellar systems that are rotating slowly. This result is based on a variety of observational and theoretical lines of evidence (Binney 1978; Davies 1987; Schechter 1987). Unfortunately, the deprojection of the surface photometry of a galaxy into a triaxial luminosity distribution is degenerate (e.g., Contopoulos 1956; Stark 1977; Rybicki 1987). Even when we require the density to be constant on similar concentric ellipsoids, the intrinsic axis ratios depend on the viewing angles, which cannot be derived from the surface photometry alone. In order to determine the intrinsic shape of an individual elliptical galaxy, additional information is needed.

There is a sizable number of elliptical galaxies that contain a gas disk or a dust lane (Hawarden *et al.* 1981; Ebneter and Balick 1985; Bertola 1987). If the gas is cold and in equilibrium it must be on simple closed orbits in the galaxy potential, which occur in a small number of preferred planes (Heiligman and Schwarzschild 1979; Gunn 1979; Tohline, Simonson, and Caldwell 1982; Habe and Ikeuchi 1985, 1988; Varnas 1986). Hence observations of the morphology and kinematics of such a gas disk can be used not only to constrain the viewing angles and the intrinsic shape of the underlying galaxy, but also to determine the mass-to-light ratio M/L as a function of radius (Merritt and de Zeeuw 1983; Gerhard and Vietri 1986, 1987).

Radial velocity measurements of ionized gas are now available for a small number of elliptical galaxies (Bertola 1987), but full use of these kinematic data has been impeded by the paucity of models for which the gas orbits and the gas velocities are known explicitly. For the determination of M/L, only spherical and axisymmetric models have been considered, with the gas assumed to be on circular orbits in the equatorial plane. For spherical systems it is trivial to deduce the gravitational potential from the rotation curve. In axisymmetric models all the stable periodic orbits lie in the equatorial plane, and hence only the potential in this plane can be determined from observations. The full potential can be derived if an ad hoc assumption is made about the two-dimensional form of either the potential or the density distribution (e.g., Burbidge, Burbidge, and Prendergast 1959; Kuzmin and Kutuzov 1966; de Zeeuw and Lynden-Bell 1988; de Zeeuw and Pfenniger 1988). In a triaxial nonrotating potential two families of stable non–self-intersecting periodic orbits occur, which lie either in the plane perpendicular to the long axis or in the plane perpendicular to the short axis. These orbits generally are not circular. This implies that the number of intrinsic parameters of a model increases, but also that there are more independent observational parameters. The analysis of the observations therefore differs considerably from the analysis of orbits in a spherical or axisymmetric potential. Detailed studies of the kinematics of gas in triaxial elliptical galaxies and bulges of spiral galaxies so far have employed numerically calculated closed orbits in triaxial potentials with given radial profiles (Gerhard and Vietri 1986, 1987; Bertola, Rubin, and Zeilinger 1989*b*; Gerhard, Vietri, and Kent 1989). It is clearly of interest to investigate in a systematic way which observational parameters are needed to determine the intrinsic shape of a triaxial galaxy, and possibly its potential, and how the dependence of the M/L ratio on radius can be derived. In this context it should be noted that the

[1] Junior Fellow, Harvard Society of Fellows.

kinematics of minor-axis gas rings in S0 galaxies have been used to infer the shape of the potential, by comparison of the rotation curve in the polar ring with that in the equatorial plane of the galaxy (Schweizer, Whitmore, and Rubin 1983; Sparke 1986; Whitmore, Schweizer, and McElroy 1987*a*, *b*). It should be worthwhile to see what other techniques may be used for this type of analysis.

In this paper we consider the special triaxial models with nonrotating figures that have a potential of Stäckel form, which form a good first-order approximation to the potentials of elliptical galaxies (Kuzmin 1973; de Zeeuw 1985*a*, hereafter Z85; Gerhard 1985; de Zeeuw, Peletier, and Franx 1986, hereafter ZPF; Franx 1988). The Hamilton-Jacobi equation separates for these systems, and hence the orbits in them can be described by analytic means. In particular, the simple closed orbits occupied by the gas are a set of confocal ellipses in the principal plane that is perpendicular either to the short axis or to the long axis of the model. The shapes of the ellipses along which the gas moves are related in a straightforward way to the shape of the galaxy. The gas velocities can be calculated analytically from the potential. This allows us to delineate in detail the kinematics of the gas when seen in projection. We analyze how the projected two-dimensional velocity field and surface density of the gas can be used to constrain the viewing angles and the mass distribution of the model, and we show that indeed in certain cases the complete intrinsic shape can be recovered. An application to the elliptical galaxy NGC 5077, which has an extended gas disk, is given by Bertola, Rubin, and Zeilinger (1989*a*).

The paper is organized in the following way. In § II the properties of gas disks and rings in Stäckel potentials are discussed. The projections of the disks and rings are studied in § III. Section IV gives an analysis of how observations of a gas ring or disk can be used to constrain the orientation of the galaxy with respect to the observer and how the intrinsic shape can be determined. In § V it is shown how the full three-dimensional potential can be derived if the aspect angles are known. The results are discussed in § VI. As it turns out, some of the principal techniques for the deprojection are independent of the assumption that the galaxy is of Stäckel form, and are applicable to all realistic galaxy potentials without figure rotation.

II. GAS DISKS IN A STÄCKEL MODEL

In this section we derive intrinsic properties of the stable gas disks in the (x, y)- and (y, z)-planes of a triaxial Stäckel model.

a) Stäckel Models

Let (x, y, z) be Cartesian coordinates, and consider a triaxial Stäckel model with its long axis in the x-direction and the short axis along the z-axis. The gravitational potential is of the form

$$V_S = -\frac{(\lambda+\alpha)(\lambda+\gamma)G(\lambda)}{(\lambda-\mu)(\lambda-\nu)} - \frac{(\mu+\alpha)(\mu+\gamma)G(\mu)}{(\mu-\nu)(\mu-\lambda)} - \frac{(\nu+\alpha)(\nu+\gamma)G(\nu)}{(\nu-\lambda)(\nu-\mu)}, \tag{2.1}$$

where (λ, μ, ν) are the usual ellipsoidal coordinates, defined as the roots for τ of

$$\frac{x^2}{\tau+\alpha} + \frac{y^2}{\tau+\beta} + \frac{z^2}{\tau+\gamma} = 1, \tag{2.2}$$

where α, β, and γ are constants with $-\gamma \le \nu \le -\beta \le \mu \le -\alpha \le \lambda$, and $G(\tau)$ is a smooth function. The foci of the ellipsoidal coordinates are at $(x, y, z) = (0, 0, \pm\Delta_1)$, $(0, 0, \pm\Delta_2)$ and at $(0, \pm\Delta, 0)$, with

$$\Delta_1^2 = \gamma - \beta, \qquad \Delta_2^2 = \gamma - \alpha, \tag{2.3}$$

and

$$\Delta^2 = \Delta_2^2 - \Delta_1^2 = \beta - \alpha. \tag{2.4}$$

Properties of the Stäckel models, their density distribution and the orbits in them, have been discussed *in extenso* by Z85 and ZPF. The latter authors also give the relation between Δ_1 and Δ_2 and the central axis ratios of the density distribution that is associated with V_S. The projected properties of Stäckel models were discussed by Franx (1988).[2]

Now consider a gas disk in equilibrium in a triaxial Stäckel model. If the gas is cold, so that the gas pressure is negligible, then the streamlines of the gas flow in the disk are identical to the stable non–self-intersecting closed orbits in the potential of the model (Tohline, Simonson, and Caldwell 1982; Steiman-Cameron and Durisen 1982). There are two families of such orbits. One family consists of elliptic closed orbits in the (x, y)-plane, while the other contains the elliptic closed orbits in the (y, z)-plane. Below, we consider their properties separately.

b) Elliptic Closed Orbits in the (x, y)-Plane

The (x, y)-plane is given by $\nu = -\gamma$. The gravitational potential in this plane is of the form

$$V_S = -\frac{(\lambda+\alpha)G(\lambda) - (\mu+\alpha)G(\mu)}{\lambda-\mu}, \tag{2.5}$$

where (λ, μ) now are elliptic coordinates, with foci at $(x, y) = (0, \pm\Delta)$. They are related to x and y by

$$\frac{x^2}{\tau+\alpha} + \frac{y^2}{\tau+\beta} = 1, \tag{2.6}$$

with $\tau = \lambda, \mu$.

[2] Our notation differs from that in Franx (1988) in one important aspect. He uses $\Delta_2^2 = \gamma - \beta$ and $\Delta_1^2 = \gamma - \alpha$, whereas we follow ZPF and use $\Delta_1^2 = \gamma - \beta$ and $\Delta_2^2 = \gamma - \alpha$.

The equations of motion in a disk with a Stäckel potential are given in Z85 (eq. [73]). In the (x, y)-plane the closed orbits lie on confocal ellipses of constant λ, which are elongated in the y-direction, i.e., perpendicular to the elongation of the density distribution of the model. On an elliptic closed orbit with $\lambda = \lambda_0$ the velocity vector is given by

$$\begin{pmatrix} v_x \\ v_y \end{pmatrix} = v_\mu \sqrt{\frac{(\lambda_0 + \alpha)(\lambda_0 + \beta)}{\lambda - \mu}} \begin{bmatrix} -y/(\lambda_0 + \beta) \\ x/(\lambda_0 + \alpha) \end{bmatrix}, \tag{2.7}$$

where v_μ is the velocity in the μ-coordinate, which in this case may be written as

$$v_\mu = \pm\sqrt{2}\sqrt{-(\mu + \alpha)\,\frac{G(\mu) - G(\lambda_0)}{\lambda_0 - \mu} - (\lambda_0 + \alpha)G'(\lambda_0)}\,. \tag{2.8}$$

The plus sign corresponds to counterclockwise motion, and the minus sign refers to clockwise motion.

For a cold gas disk, the surface density Σ_g and the velocity field of the gas are connected by the equation of continuity,

$$\nabla \cdot \Sigma_g \boldsymbol{v} = 0\,. \tag{2.9}$$

Expressed in (λ, μ), this becomes

$$\frac{1}{PQ}\left(\frac{\partial}{\partial\lambda} Q\Sigma_g v_\lambda + \frac{\partial}{\partial\mu} P\Sigma_g v_\mu\right) = 0\,, \tag{2.10}$$

where P and Q are the metric coefficients of the elliptic coordinates, given in equation (5) of Z85. Since the gas streams along lines of constant λ, we have $v_\lambda \equiv 0$, and we are left with

$$P\Sigma_g v_\mu = \text{constant}\,. \tag{2.11}$$

As a result, the gas surface density Σ_g at a general point is given by

$$\Sigma_g(\lambda, \mu) = \Sigma_g(\lambda, -\alpha)\,\frac{v_\mu(\lambda, -\alpha)}{v_\mu(\lambda, \mu)}\sqrt{\frac{\lambda + \alpha}{\lambda - \mu}}\,, \tag{2.12}$$

where v_μ is given in equation (2.8). The function $\Sigma_g(\lambda, -\alpha)$ is equal to the surface density of the gas along the y-axis beyond the foci ($|y| \geq \Delta$), and can be chosen arbitrarily. The other terms in equation (2.12) determine the two-dimensional distribution of the gas. For constant λ both the factor with the square root and the velocity v_μ are smallest for $\mu = -\alpha$, i.e., along the y-axis. Hence along each ellipse of constant λ the density is greatest at the intersection with the y-axis. We note that the piece of the y-axis between the foci is given by $\lambda = -\alpha$. If we require $\Sigma_g(\lambda, -\alpha)$ to be everywhere finite, the density will be zero there. The velocity field is discontinuous along this part of the y-axis.

As an example, we have calculated the velocity field in the (x, y)-plane of the potential of the perfect ellipsoid. This is the prototypical Stäckel model (Kuzmin 1973; Z85), and is discussed briefly in § III*d*. The appropriate function $G(\tau)$ is given in equation (B9) of Z85 and can easily be evaluated numerically. The resulting velocity field is shown in Figure 1*a*. Figure 1*b* shows contours of constant projected surface density of the gas for the choice

$$\Sigma_g(\lambda, -\alpha) = \frac{\sqrt{\lambda + \alpha}}{\lambda}\,. \tag{2.13}$$

The gas density along the y-axis is zero up to the foci, then increases to a maximum for $y^2 = -2\alpha + \beta$, and subsequently decreases as $1/\sqrt{\lambda} \sim 1/y$ at large y. It can be seen in Figure 1*b* that at intermediate and large radii, the surface density of the gas is elongated perpendicular to the density distribution which produces the potential. Note that at large radii the isophotes of the gas surface density do not become round as quickly as the λ coordinate lines.

c) *Elliptic Closed Orbits in the* (y, z)*-Plane*

Now we consider a gas disk in the (y, z)-plane. In ellipsoidal coordinates this plane is defined by $\lambda = -\alpha$ or $\mu = -\alpha$. We denote the coordinate which is unequal to $-\alpha$ by κ. Equation (2.5) describes the potential in this plane if we transform (x, y), (λ, μ), and (α, β) to (y, z), (κ, ν), and (β, γ) via

$$x \to y\,, \quad y \to z\,, \quad \alpha \to \beta\,, \quad \beta \to \gamma\,, \quad \mu \to \nu\,, \quad \lambda \to \kappa\,, \tag{2.14}$$

and replace $G(\tau)$ in equation (2.5) by $(\tau + \gamma)G(\tau)/(\tau + \beta)$. All the properties of the gas disk then follow immediately from those given in § II*b*.

The velocity vector on the ellipse $\kappa = \kappa_0$ in the (y, z)-plane can be written as

$$\begin{pmatrix} v_y \\ v_z \end{pmatrix} = v_\nu \sqrt{\frac{(\kappa_0 + \beta)(\kappa_0 + \gamma)}{\kappa_0 - \nu}} \begin{bmatrix} -z/(\kappa_0 + \gamma) \\ y/(\kappa_0 + \beta) \end{bmatrix}, \tag{2.15}$$

where v_ν, the velocity in ν, is given by

$$v_\nu = \pm\sqrt{2}\sqrt{-(\nu + \gamma)\,\frac{G(\nu) - G(\kappa_0)}{\kappa_0 - \nu} - (\kappa_0 + \gamma)G'(\kappa_0)}\,. \tag{2.16}$$

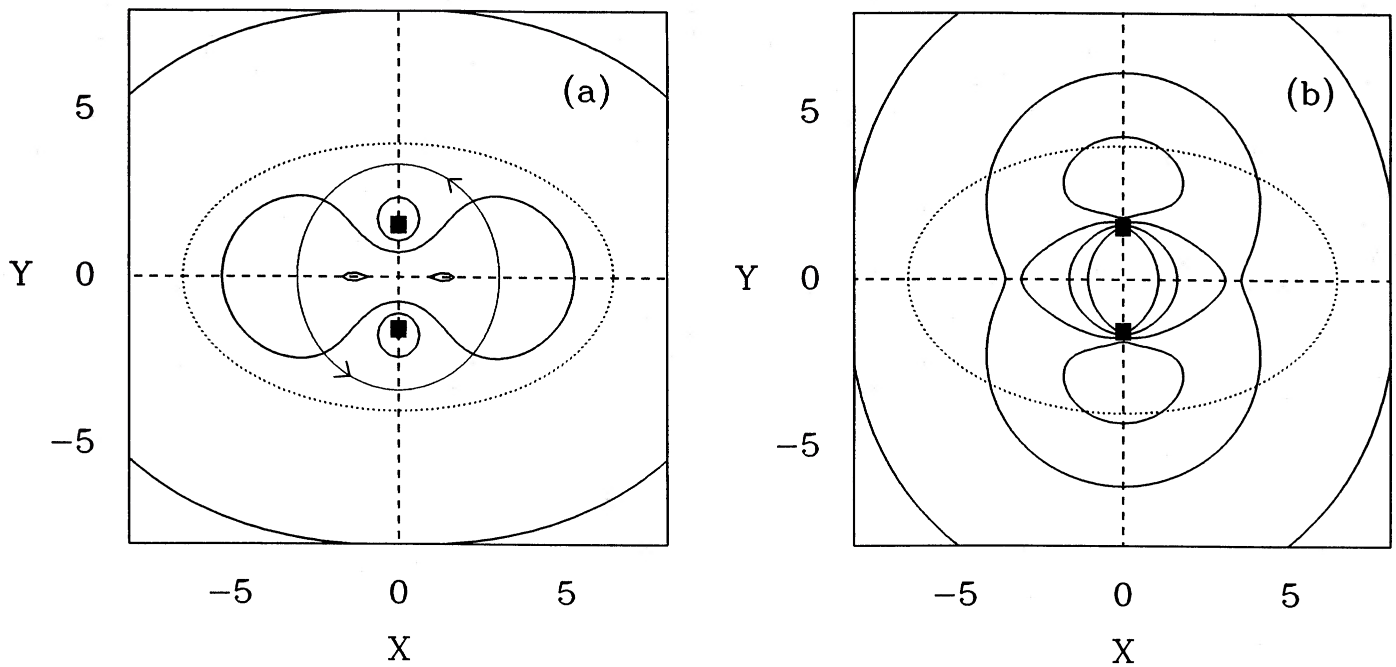

FIG. 1.—(*a*) Velocity field of gas on the elliptic closed orbits in the (x, y)-plane of the perfect ellipsoid with axis ratios 1:0.625:0.5. Contours of constant velocity are drawn at linear intervals in the orbital velocity v_μ. The velocity reaches its maximum along the x-axis, and decreases to zero at the foci, which are denoted by the filled squares. The dotted ellipse is a contour of constant stellar density. The thin-drawn ellipse with the arrows, which is elongated along the y-axis, is a closed orbit. (*b*) Contours of constant gas density, for the assumed minor-axis density $\Sigma_g(\lambda, -\alpha)$ of eq. (2.13). The contours are at linear intervals. The surface density is zero in the center, and has a maximum along the y-axis.

By means of the equation of continuity, we find for the surface density of the disk

$$\Sigma_g(\kappa, \nu) = \Sigma_g(\kappa, -\beta)\,\frac{v_\nu(\kappa, -\beta)}{v_\nu(\kappa, \nu)}\sqrt{\frac{\kappa+\beta}{\kappa-\nu}}\,, \tag{2.17}$$

where $\Sigma_g(\kappa, -\beta)$ is the surface density along the z-axis beyond the foci at $z = \pm\Delta_1$.

d) Validity of Approach

Numerical simulations using smooth-particle hydrodynamics (Habe and Ikeuchi 1985; Varnas 1986) have shown that in a nonrotating triaxial galaxy infalling gas settles in a symmetry plane on a time scale of a few times 10^9 yr. Depending on the initial angular momentum of the gas, the gas settles either in the plane perpendicular to the long axis or in the plane perpendicular to the short axis. In these planes, the gas follows the simple closed orbits to good accuracy, and it forms a ring or disk that is stable for many dynamical times. These results are in agreement with the analytic description of the settling process by Steiman-Cameron and Durisen (1982, 1988).

Since the gas does not move along circles, but rather along ellipses in the symmetry planes of the potential, one might worry that shocks will occur near the minima of the potential along a streamline. The shapes of the periodic orbits may be used to predict the occurrence of shocks (e.g., van Albada and Sanders 1982). Since the simple closed orbits in a nonrotating triaxial galaxy are nested, and nonintersecting, shocks are not expected to occur, except in the region near the foci. There many streamlines come together, and hence a significant pressure can build up. Furthermore, the velocity field is discontinuous on the part of the principal axis between the foci, hence shocks will occur almost certainly in that region. Note that this will be the case not only for triaxial galaxies with a separable potential, in which the simple closed orbits are exact confocal ellipses, but also in general nonrotating triaxial systems with a finite core radius. In the latter case the simple closed orbits are only approximately elliptic, but they also become highly elongated in the central region, and join with the oscillations along a principal axis at a finite amplitude (Heiligman and Schwarzschild 1979). The velocity field is therefore discontinuous along this axis between the bifurcation points, so that shocks are again expected to occur here. The possible connection of this behavior with the feeding of a central "monster" has been discussed by Gunn (1979).

We therefore conclude that the assumption that the gas is on closed orbits is not valid in the central regions of a triaxial galaxy. However, on the basis of the numerical experiments mentioned earlier, we expect that the closed-orbit approximation is accurate in the regions where the velocity dispersion of the gas is small compared with the orbital velocity, and where the orbits are not too strongly elongated. In these regions the velocity fields calculated from the simple closed orbits should give an adequate description of the gas kinematics.

III. PROJECTED PROPERTIES

We now project the gas disks of § II along a line of sight in an arbitrary direction, and consider the observable properties.

a) Notation

Franx (1988) has studied the projected density distribution of Stäckel models in detail. We follow his notation, and choose new coordinates (x'', y'', z''), with the z''-axis along the line of sight, and with the x''-axis in the (x, y)-plane (see also Binney 1985). The disk is projected onto the (x'', y'')-plane. Let ϑ and φ be the standard spherical polar angles of the z''-axis in the (x, y, z) coordinates. The coordinate transformation is

$$\begin{pmatrix} x \\ y \\ z \end{pmatrix} = \begin{pmatrix} -\sin\varphi & -\cos\varphi\cos\vartheta & \cos\varphi\sin\vartheta \\ \cos\varphi & -\sin\varphi\cos\vartheta & \sin\varphi\sin\vartheta \\ 0 & \sin\vartheta & \cos\vartheta \end{pmatrix} \begin{pmatrix} x'' \\ y'' \\ z'' \end{pmatrix}. \tag{3.1}$$

The inverse transformation is

$$\begin{pmatrix} x'' \\ y'' \\ z'' \end{pmatrix} = \begin{pmatrix} -\sin\varphi & \cos\varphi & 0 \\ -\cos\varphi\cos\vartheta & -\sin\varphi\cos\vartheta & \sin\vartheta \\ \cos\varphi\sin\vartheta & \sin\varphi\sin\vartheta & \cos\vartheta \end{pmatrix} \begin{pmatrix} x \\ y \\ z \end{pmatrix}. \tag{3.2}$$

As a result, the z-axis projects onto the y''-axis. In what follows, *all position angles are taken with respect to the y''-axis, in counterclockwise direction, and are denoted by the symbol Θ*. The position angle Θ_z of the projected z-axis is therefore equal to zero. The position angles Θ_x and Θ_y of the projected x-axis and y-axis, respectively, are given by

$$\tan\Theta_x = -\frac{\sin\varphi}{\cos\varphi\cos\vartheta}, \qquad \tan\Theta_y = \frac{\cos\varphi}{\sin\varphi\cos\vartheta}. \tag{3.3}$$

An observer will not know the direction of one of the projected symmetry axes *a priori*, and measures position angles with respect to the north. These we denote by the symbol $\hat{\Theta}$. We introduce an extra angle of projection χ, which is the position angle $\hat{\Theta}_z$ of the projected z-axis (i.e., the y''-axis) with respect to the north. The two sets of angles are related by

$$\hat{\Theta} = \Theta + \chi. \tag{3.4}$$

Figure 2 illustrates the two coordinate systems (x, y, z) and (x'', y'', z'') as well as our convention for the various angles.

b) Gas in the (x, y)-Plane

The projection (x'', y'') of a point $(x, y, 0)$ in the (x, y)-plane can be found by means of equation (3.2). The inverse relation between $(x, y, 0)$ and (x'', y'') is

$$x = -x''\sin\varphi - y''\frac{\cos\varphi}{\cos\vartheta}; \qquad y = x''\cos\varphi - y''\frac{\sin\varphi}{\cos\vartheta}. \tag{3.5}$$

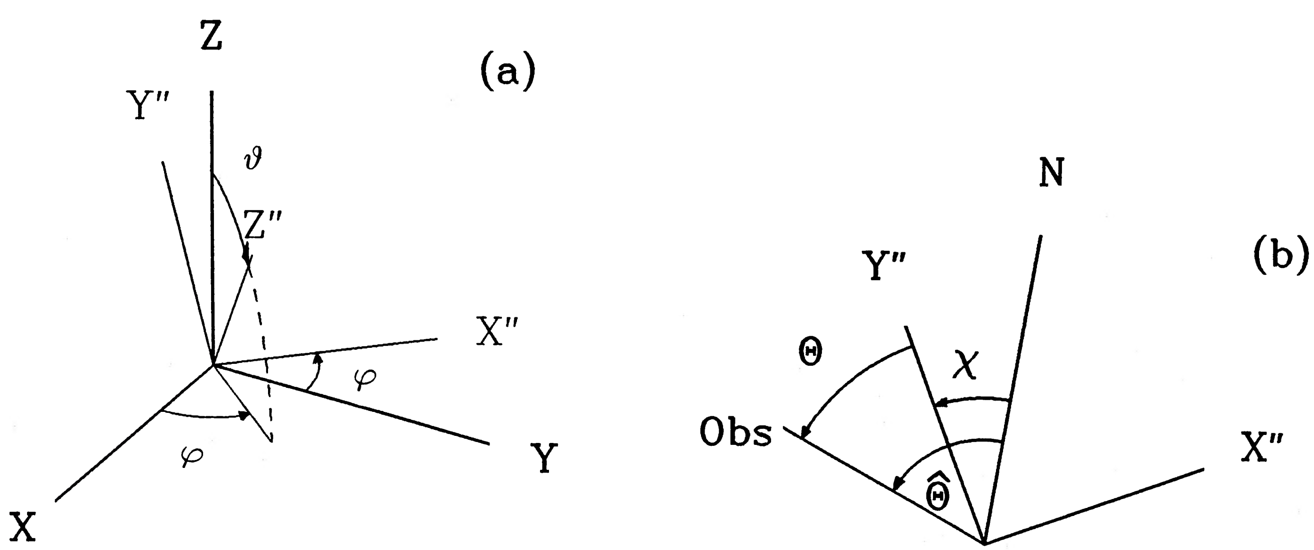

FIG. 2.—(*a*) Coordinate systems used for projection. The angles ϑ and φ define the direction of the line of sight, which is taken to be the z''-axis. (*b*) Angles in the plane of the sky [i.e., the (x'', y'')-plane]. See text for further details.

Since $v_z = 0$, the line-of-sight velocity $\dot{z}''$ is equal to v_r, with (cf. eq. [3.2])

$$v_r = v_x \cos \varphi \sin \vartheta + v_y \sin \varphi \sin \vartheta , \tag{3.6}$$

or, upon substitution of equation (2.7),

$$v_r = v_\mu \sin \vartheta \frac{-(\lambda_0 + \alpha)y \cos \varphi + (\lambda_0 + \beta)x \sin \varphi}{\sqrt{(\lambda_0 + \alpha)(\lambda_0 + \beta)(\lambda_0 - \mu)}} . \tag{3.7}$$

This gives the value of v_r at the point (x'', y'') that corresponds to the point on the elliptic closed orbit with Cartesian coordinates (x, y), or the equivalent elliptic coordinates (λ_0, μ).

As an example, we have calculated the projected velocity field for the disk of Figure 1, for a direction of observation given by $\vartheta = 60°$ and $\varphi = 45°$. The result is shown in Figure 3*a*. It is evident from the figure that if we observe the radial velocities along a given position angle, which would be the case with single-slit spectroscopy, then the amplitude and shape of the derived "rotation curve" depend on the position angle of the slit and on the viewing angles of the disk (Gerhard and Vietri 1986). Teuben (1987) has discussed this in the context of a specific Stäckel model. In Figure 4 we illustrate a number of these "rotation curves." If we happen to observe along the projected x-axis, the rotation curve will approach a finite (nonzero) value in the center, where it is formally discontinuous (Fig. 4*a*). Along the position angle Θ_y of the projected y-axis, the rotation curve will be zero out to a finite radius (Fig. 4*b*). The observed radial velocities at the major and minor axes of the projected stellar density distribution are presented in Figures 4*c* and 4*d*. Since the orbits are noncircular, the curve of zero radial velocity is not a straight line in the plane of projection. Hence the observed radial velocity along a slit may change sign outside the center. This is clearly visible in Figure 4*d*. We remark that in panels *a* and *b*, positive coordinates along the horizontal axis correspond to positive coordinates along the x- and y-axis, respectively. However, the position angles of the major and minor axis are constrained to lie between $-\pi/2$ and $+\pi/2$ (see § III*d*). As a result, the positive values along the horizontal axis in panel *c* correspond to the piece of the apparent major axis with negative x'' and y'', i.e., in the lower left-hand corner of Figure 3*a*. This causes the apparent change of sign between panels *a* and *c*.

The projected surface density of the gas can be calculated easily with the help of equations (2.6), (2.12), and (3.5). Figure 3*b* gives an example of the projection of the density drawn in Figure 1. It is evident that the position angles of the isodensity contours change with radius. The way in which they do so depends on the specific form of the function $\Sigma_g(\lambda, -\alpha)$, which, as we have seen, is the gas density along the y-axis.

i) *Zero-Velocity Curve*

In order to derive the observed zero-velocity curve, we first determine the locus of points in the (x, y)-plane where the velocity is perpendicular to the line of sight. Equations (2.6) and (3.7) imply that this curve is a solution of

$$-(\lambda_0 + \alpha)y \cos \varphi + (\lambda_0 + \beta)x \sin \varphi = 0 , \tag{3.8a}$$

$$\frac{x^2}{\lambda_0 + \alpha} + \frac{y^2}{\lambda_0 + \beta} = 1 . \tag{3.8b}$$

We use equation (3.8a) to express λ_0 as a function of x, y and φ, and insert the result in equation (3.8b). This produces

$$-x^2 + xy(\cot \varphi - \tan \varphi) + y^2 = (\beta - \alpha) = \Delta^2 . \tag{3.9}$$

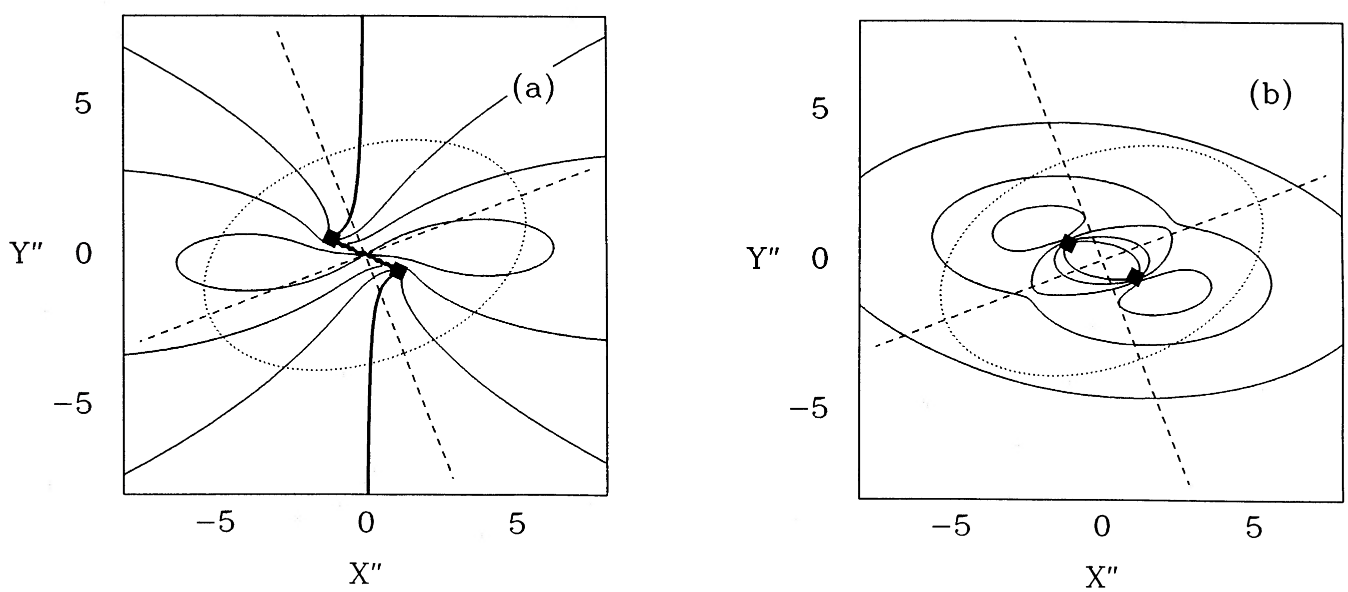

FIG. 3.—(*a*) Projected velocity field of the gas disk of Fig. 1, for viewing angles $\vartheta = 60°$ and $\varphi = 45°$. Contours of constant radial velocity are drawn at linear intervals. The thick curve is the curve of zero radial velocity. The filled squares denote the foci. The dotted ellipse is a contour of constant projected surface density of the stars. The principal axes of the projected stellar density distribution are indicated by the dashed lines. (*b*) Contours of constant projected gas density for the same model.

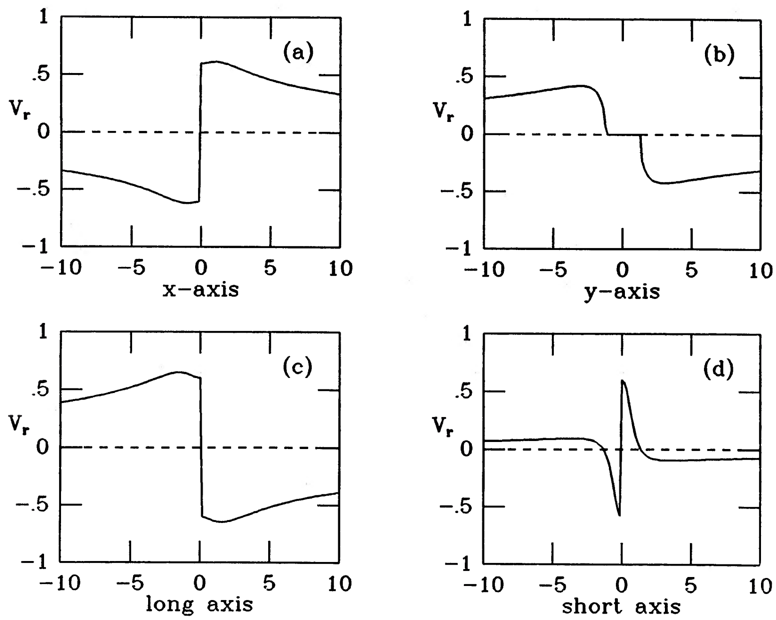

FIG. 4.—Rotation curves as observed along different directions. (*a*) Along the projected *x*-axis. (*b*) Along the projected *y*-axis. (*c*) Along the apparent major axis of the projected density distribution. (*d*) Along the apparent minor axis of the projected density distribution. Further details are given in the text.

This curve is a hyperbola, which runs through the foci at $(x, y) = (0, \pm\Delta)$. The asymptotes are perpendicular to each other, with one perpendicular to the line of sight and the other parallel to the projected line of sight in the (x, y)-plane. Along the hyperbola either the λ or the μ coordinate line is perpendicular to the line of sight. The lines of constant λ are perpendicular to the line of sight, and hence $v_r = 0$, for all points along the hyperbola with

$$\frac{x \sin \varphi}{y \cos \varphi - x \sin \varphi} \geq 0 . \tag{3.10}$$

The above result gives the zero-velocity curve in the (x, y)-plane for all values of $\vartheta > 0$. If $\vartheta = 0$, then the radial velocity is zero everywhere in the (x, y)-plane. We use equation (3.5) to replace (x, y) by (x'', y'') in equations (3.9) and (3.10), and we obtain for the zero-velocity curve in the (x'', y'')-plane

$$x''y'' = -(\beta - \alpha) \sin \varphi \cos \varphi \cos \vartheta , \tag{3.11a}$$

$$y''^2 \geq (\beta - \alpha) \sin^2 \varphi \cos^2 \vartheta . \tag{3.11b}$$

For a general direction of viewing, equation (3.11) describes two parts of a hyperbola, with the x''- and y''-axes as asymptotes. The radial velocity is zero at the parts of the hyperbola for which $|y''| \geq \Delta \sin \varphi \cos \vartheta$, so that $|x''| \leq \Delta \cos \varphi$. These limits correspond to $\lambda_0 = -\alpha$, for which the orbit is the y-axis oscillation between the foci at $y = \pm\Delta$. It follows that v_r changes sign on the projected y-axis for all values of y'' which satisfy $|y''| \leq \Delta \sin \varphi \cos \vartheta$, as can be seen in Figure 3*a*. Thus, this part of the projected y-axis belongs to the zero-velocity curve, and connects the two branches of the hyperbola (3.11).

If $\vartheta = 0$, we see the disk face-on, and the radial velocity is zero everywhere. In case $\vartheta = \pi/2$, we see the disk edge-on, and the radial velocity is zero at $x'' = y'' = 0$. When the direction of observation lies in the principal plane perpendicular to the x-axis or to the principal plane perpendicular to the y-axis, we have either $\sin \varphi = 0$ or $\cos \varphi = 0$, so that the zero-velocity curve becomes a straight line which coincides with the y''-axis. In this case either the minor axis or the major axis of the projected surface density distribution of the stars is in the direction of the y''-axis (see § III*d*). Finally, for $\Delta = 0$ the model becomes axisymmetric. In this case the elliptic closed orbits in the (x, y)-plane reduce to circular orbits in the equatorial plane of the model. The zero-velocity curve is identical to the y''-axis for any direction of viewing.

It should be noted that *the equation for the zero-velocity curve contains only the viewing angles ϑ and φ, and $\beta - \alpha$. It is independent of $G(\tau)$, and hence independent of the detailed density distribution of the model.* It follows that the zero-velocity curve of a gas disk can give useful constraints on the viewing angles, irrespective of the behavior of M/L. This will be discussed in detail in § IV.

The velocity field also has a maximum velocity curve, which is the curve on which the radial velocity has a zero derivative in the direction perpendicular to the curve. This curve is determined, however, by both the geometry of the coordinate system (λ, μ) and the specific form of the function $G(\tau)$. Hence it is less convenient to use in the determination of the viewing angles ϑ and φ from the observations.

ii) *Projection of a Single Orbit*

We now discuss in more detail the case where the gas is orbiting on a single ellipse (2.6), with $\tau = \lambda_0$. This ellipse projects to another ellipse, irrespective of the distribution of gas along the orbit. The situation is illustrated in Figure 5. The projected major-

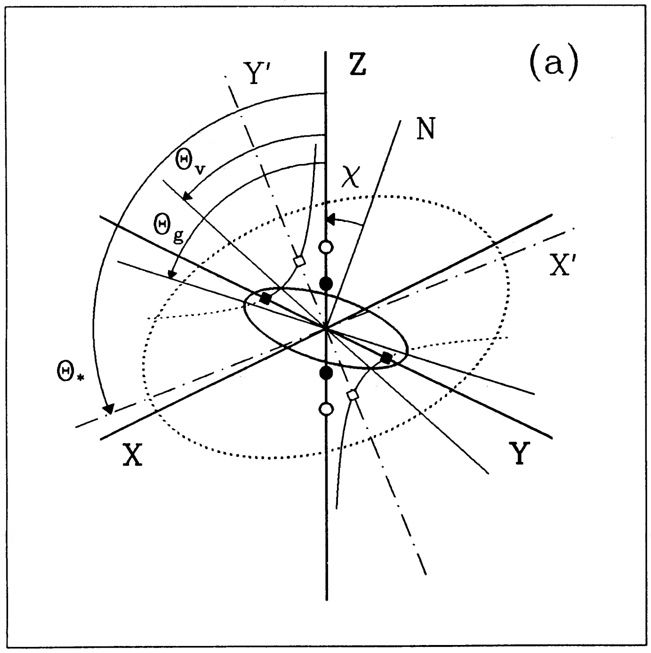

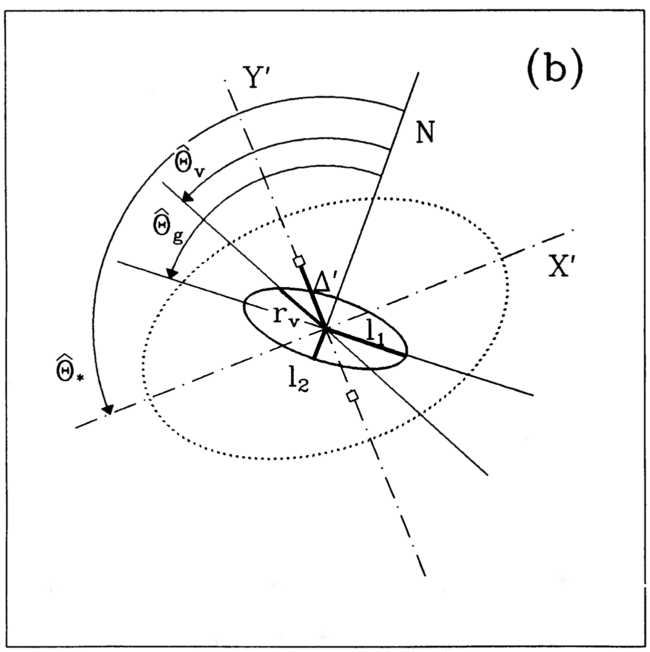

FIG. 5.—(*a*) Projection of a single elliptic orbit in the (x, y)-plane. The angles are defined in the text. The inner, full ellipse is the gas ellipse. The thick lines are the projected principal axes of the model. The filled squares are the foci of the elliptic closed orbits in the (x, y)-plane, while the filled circles are the foci of the elliptic closed orbits in the (y, z)-plane, and the open circles are the foci of the unstable elliptic closed orbits in the (x, z)-plane. The zero-velocity hyperbola intersects the foci of the projected ellipse, the projected foci on the y-axis (*filled squares*), and the zero-velocity points on the gas ellipse. The x'- and y'-axes, which are the principal axes of the projected stellar density distribution, are indicated by the dash-dot lines. The associated foci are indicated by open squares. The dotted ellipse is a contour of constant projected stellar density. (*b*) Observable parameters, as defined in the text. The angles are measured with respect to the north. The thick-drawn line pieces are the observational scale parameters.

and minor-axis lengths l_1 and l_2 follow immediately from formula (B7) and (B8) of Franx (1988):

$$l_1^2 = \tfrac{1}{2}(d_1 + d_2) , \qquad l_2^2 = \tfrac{1}{2}(d_1 - d_2) , \tag{3.12}$$

with

$$\begin{aligned} d_1 &= l^2(1 + \cos^2 \vartheta) + (\beta - \alpha)(\cos^2 \varphi + \sin^2 \varphi \cos^2 \vartheta) , \\ d_2^2 &= [l^2 \sin^2 \vartheta + (\beta - \alpha)(\cos^2 \varphi - \sin^2 \varphi \cos^2 \vartheta)]^2 + 4(\beta - \alpha)^2 \sin^2 \varphi \cos^2 \varphi \cos^2 \vartheta , \end{aligned} \tag{3.13}$$

and we have written $l^2 = \lambda_0 + \alpha$, so that l is the intrinsic semiminor-axis length of the ellipse. The position angle $\Theta_{\rm gas}$ of the ellipse, defined as the angle between the direction of the apparent major axis l_1 and the y''-axis, is given by (Franx 1988, eq. [B9])

$$\tan 2\Theta_{\rm gas} = - \frac{2(\beta - \alpha) \sin \varphi \cos \varphi \cos \vartheta}{l^2 \sin^2 \vartheta + (\beta - \alpha)(\cos^2 \varphi - \sin^2 \varphi \cos^2 \vartheta)} , \tag{3.14}$$

with

$$(\beta - \alpha) \sin 2\Theta_{\rm gas} \sin 2\varphi \cos \vartheta \ge 0 \qquad \text{and} \qquad -\pi/2 < \Theta_{\rm gas} \le \pi/2 . \tag{3.15}$$

The foci of the projected ellipse lie at a distance of $(l_1^2 - l_2^2)^{1/2}$ from the center, at position angles $\Theta_{\rm gas}$ and $\Theta_{\rm gas} + \pi$. It is not difficult to show that these foci lie on the hyperbola defined in equation (3.11a), but on the parts that do not satisfy the condition (3.11b).

The angle $\Theta_{\rm gas}$ and the axis ratio l_2/l_1 of the projected orbit are both functions of l. As l increases, the orbits become more nearly circular, and the position angle and ellipticity of the projected orbit will approach the angle and ellipticity of a projected circle, i.e., $\Theta_{\rm gas} \to 0$ for $l \to \infty$, and $l_2/l_1 \to \cos \vartheta$. For $l = 0$, i.e., $\lambda_0 = -\alpha$, the orbit is the y-axis oscillation between the foci at $y = \pm\Delta$. By equation (3.2) these points project to $(x'', y'') = (\pm\Delta \cos \varphi, \pm\Delta \sin \varphi \cos \vartheta)$, so that $\Theta_{\rm gas} = \Theta_y$.

The observed radial velocity is zero at two points on the orbit, which are of course given by the intersection of the projected orbit with the zero-velocity curve (3.11). These points are located at

$$x'' = \pm \frac{(\beta - \alpha) \sin \varphi \cos \varphi}{\sqrt{l^2 + (\beta - \alpha) \sin^2 \varphi}} , \qquad y'' = \mp \cos \vartheta \sqrt{l^2 + (\beta - \alpha) \sin^2 \varphi} , \tag{3.16}$$

so that they have position angles Θ_v and $\Theta_v + \pi$ with respect to the y''-axis, given by

$$\tan \Theta_v = \frac{(\beta - \alpha) \sin \varphi \cos \varphi}{[l^2 + (\beta - \alpha) \sin^2 \varphi] \cos \vartheta} . \tag{3.17}$$

Thus, $x'' = -r_v \sin \Theta_v$ and $y'' = r_v \cos \Theta_v$, with $r_v^2 = x''^2 + y''^2$. Since these points lie on the zero-velocity curve (3.11), we have the relation

$$r_v^2 \sin 2\Theta_v = 2(\beta - \alpha) \sin \varphi \cos \varphi \cos \vartheta . \tag{3.18}$$

At the zero radial velocity points the intrinsic velocity vector is parallel to the plane of projection, and hence is parallel to the tangent of the projected ellipse at these points. As a result, this tangent is perpendicular to the y''-axis, and hence there is a relation between the position angles $\Theta_{\rm gas}$ and Θ_v. This relation can be derived as follows. Let (x_g, y_g) be the Cartesian coordinates in which the projected ellipse has the normal form

$$\frac{x_g^2}{l_1^2} + \frac{y_g^2}{l_2^2} = 1 , \tag{3.19}$$

so that the zero-velocity points have the coordinates

$$x_g = \pm r_v \cos (\Theta_v - \Theta_{\rm gas}) , \qquad y_g = \pm r_v \sin (\Theta_v - \Theta_{\rm gas}) , \tag{3.20}$$

where $r_v^2 = x''^2 + y''^2 = x_g^2 + y_g^2$. Since the tangent vector at these points is given by $(\mp y_g l_1^2, \pm x_g l_2^2)$, the y''-axis is parallel to the vector $(x_g l_2^2, y_g l_1^2)$, and hence we have

$$\tan \Theta_{\rm gas} = \frac{l_1^2}{l_2^2} \tan (\Theta_{\rm gas} - \Theta_v) , \tag{3.21}$$

which is the desired relation.

The angle $\Theta_v - \Theta_{\rm gas} + \pi/2$ is the difference between the position angle of the apparent minor axis of the ellipse and the zero radial velocity point. Figure 6 shows contours of constant $\Theta_v - \Theta_{\rm gas} + \pi/2$ on the unit sphere of projection directions for a gas ring with major-axis length $l_1 = 1.85$ and minor-axis length $l_2 = 1.0$. From this example it is evident that the position angle of the zero-velocity point may differ significantly from the minor-axis position angle of the projected ellipse.

Finally, we remark that the hyperbola (3.11a) intersects the projected ellipse at two additional points, with coordinates

$$x'' = \pm \sqrt{l^2 + (\beta - \alpha) \cos^2 \varphi} , \qquad y'' = \mp \frac{(\beta - \alpha) \sin \varphi \cos \varphi \cos \vartheta}{\sqrt{l^2 + (\beta - \alpha) \cos^2 \varphi}} \tag{3.22}$$

At these points the tangent to the ellipse is parallel to the y''-axis.

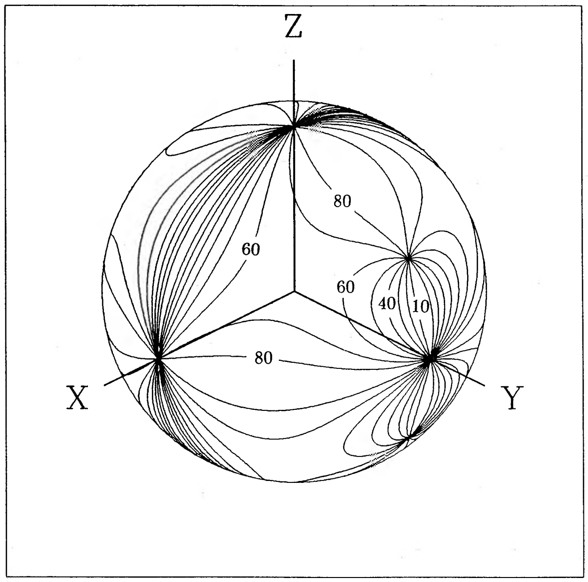

FIG. 6.—Position-angle difference $\Theta_v - \Theta_{gas} + \pi/2$ between the direction of the zero-velocity point and the minor axis of a projected gas ring with semiaxis lengths $l_1 = 1.85$ and $l_2 = 1.0$ in a perfect ellipsoid with axis ratios 0.5:0.625:1.0. Contours of constant difference are drawn at intervals of 10° on the unit sphere of projection directions.

c) *Gas in the* (y, z)*-Plane*

The projected properties of a gas disk in the (y, z)-plane can be derived from those given in § III*b* for a disk in the (x, y)-plane by use of the transformation (2.14) to change from (x, y) to (y, z). In order to have the y''-axis coincide with the projected z-axis, the coordinate system (x'', y'') defined in equation (3.5) must be rotated over an angle Θ_y. The angle ϑ then is again the inclination of the disk, and φ is an azimuthal angle in the plane of the disk. All observed properties now follow from the relevant equations of § III*b*.

In practice it is useful to have explicit expressions for the projected properties of the disk in the (y, z)-plane in the same coordinates used in the discussion of the (x, y)-plane. These can be derived by direct calculation, or by application of the above-mentioned procedure to the equations given in § III*b*. If we then rename the angles ϑ and φ to i and ϕ, respectively, and subsequently use the transformation

$$\cos i = \sin \vartheta \cos \varphi \, , \qquad \tan \phi = \frac{\cos \vartheta}{\sin \vartheta \sin \varphi} \, , \tag{3.23}$$

we obtain the desired expressions. We summarize the main results. The coordinates $(0, y, z)$ are related to the coordinates (x'', y'') in the plane of projection by (cf. eq. [3.1])

$$y = \frac{x''}{\cos \varphi} \, , \qquad z = x'' \tan \varphi \cot \vartheta + \frac{y''}{\sin \vartheta} \, . \tag{3.24}$$

The radial velocity v_r at a point (x'', y'') is given by

$$v_r = v_v \frac{(\kappa_0 + \gamma)y \cos \vartheta - (\kappa_0 + \beta)z \sin \varphi \sin \vartheta}{\sqrt{(\kappa_0 + \beta)(\kappa_0 + \gamma)(\kappa - \nu)}} \, , \tag{3.25}$$

where v_v is given in equation (2.16), and (κ_0, ν) are the elliptic coordinates of the point (y, z).

i) *Zero-Velocity Curve*

The zero-velocity curve in the coordinates (x'', y'') is given by

$$y''^2 - x''^2 + \frac{\sin^2 \varphi - \cos^2 \varphi \cos^2 \vartheta}{\sin \varphi \cos \varphi \cos \vartheta} x''y'' = (\gamma - \beta) \sin^2 \vartheta \, , \tag{3.26a}$$

$$\frac{x'' \cos \varphi \cos \vartheta}{y'' \sin \varphi - x'' \cos \vartheta \cos \varphi} \geq 0 \, . \tag{3.26b}$$

This is the equation of a hyperbola which has one of its asymptotes at position angle Θ_x, i.e., along the projected x-axis, and the other at $\Theta_x + \pi/2$. As a result, $v_r = 0$ for an arbitrary point (x'', y'') in case $\vartheta = \pi/2$ and $\varphi = 0$ or π, so that we see the (y, z)-plane exactly face-on. In case $\vartheta = 0$ or π, we observe the disk edge-on, and $v_r = 0$ for $x'' = y'' = 0$.

Excluding these special cases, the line-of-sight velocity is zero on the points given in equation (3.26). For a general direction of viewing, and for $\gamma - \beta = \Delta_1^2 \neq 0$, so that the model is not prolate, $v_r = 0$ for the parts of the hyperbola that obey the condition

(3.26b). The limits correspond to $\kappa_0 = -\beta$, for which the orbit is the z-axis oscillation between the foci at $z = \pm\Delta_1$. At the two sides of the y''-axis for $|y''| \leq \Delta_1 \sin \vartheta$ the radial velocities have different signs, and it follows that we will measure $v_r = 0$ on this part of the y''-axis, which therefore is also a part of the zero-velocity curve.

If the direction of observation lies in the (x, y)-plane, the zero-velocity curve becomes a straight line which coincides with the x''-axis. In this case the major axis of the projected density distribution is in the same direction. If the direction of projection lies in the (y, z)-plane, the disk projects to a line. If the direction of observation lies in the (x, z)-plane, the zero-velocity curve coincides with the y''-axis. Finally, for $\gamma = \beta$ the model is prolate. The elliptic closed orbits in the (y, z)-plane now reduce to the circular orbits in the equatorial plane. The zero velocity curve is identical to the x''-axis for an arbitrary direction of viewing. In Figure 7*a* we show an example of the velocity field of a projected gas disk in the (y, z)-plane of the model used in Figure 1. The associated projected surface density of the gas is shown in Figure 7*b*.

ii) *Projection of a Single Orbit*

The ellipse $\kappa = \kappa_0$ in the (y, z)-plane projects to an ellipse in the (x'', y'')-plane with semimajor- and semiminor-axis lengths k_1, k_2, given by

$$k_1^2 = \tfrac{1}{2}(d_1 + d_2)\,, \qquad k_2^2 = \tfrac{1}{2}(d_1 - d_2)\,, \tag{3.27}$$

with

$$d_1 = k^2(1 + \cos^2\varphi \sin^2\vartheta) - (\gamma - \beta)\sin^2\vartheta\,,$$
$$d_2^2 = [k^2(\sin^2\varphi - \cos^2\varphi\cos^2\vartheta) + (\gamma - \beta)\sin^2\vartheta]^2 + 4k^4\sin^2\varphi\cos^2\varphi\cos^2\vartheta\,, \tag{3.28}$$

and where we have written $k^2 = \kappa_0 + \beta$, so that k is the semiminor-axis length of the original ellipse. The position angle $\Theta_{\rm gas}$ of the ellipse—the angle between the major axis k_1 and the projected z-axis—is given by

$$\tan 2\Theta_{\rm gas} = \frac{2k^2 \sin\varphi\cos\varphi\cos\vartheta}{k^2(\sin^2\varphi - \cos^2\varphi\cos^2\vartheta) + (\gamma - \beta)\sin^2\vartheta}\,, \tag{3.29}$$

with

$$k^2 \sin 2\Theta_{\rm gas} \sin 2\varphi \cos\vartheta \geq 0 \qquad \text{and} \qquad -\frac{\pi}{2} < \Theta_{\rm gas} \leq \frac{\pi}{2}\,. \tag{3.30}$$

As k increases, the orbits become more nearly circular, and $\Theta_{\rm gas} \to \Theta_x + \pi/2$, $k_2/k_1 \to \cos\varphi \sin\vartheta$ for $k \to \infty$. For $k = 0$, i.e., for $\kappa_0 \to -\beta$, the orbit approaches the z-axis oscillation between the foci at $z = \pm\Delta_1$. These foci project to $(x'', y'') = (0, \pm\Delta_1 \sin\vartheta)$, so that in this limit $\Theta_{\rm gas} \to \Theta_z = 0$.

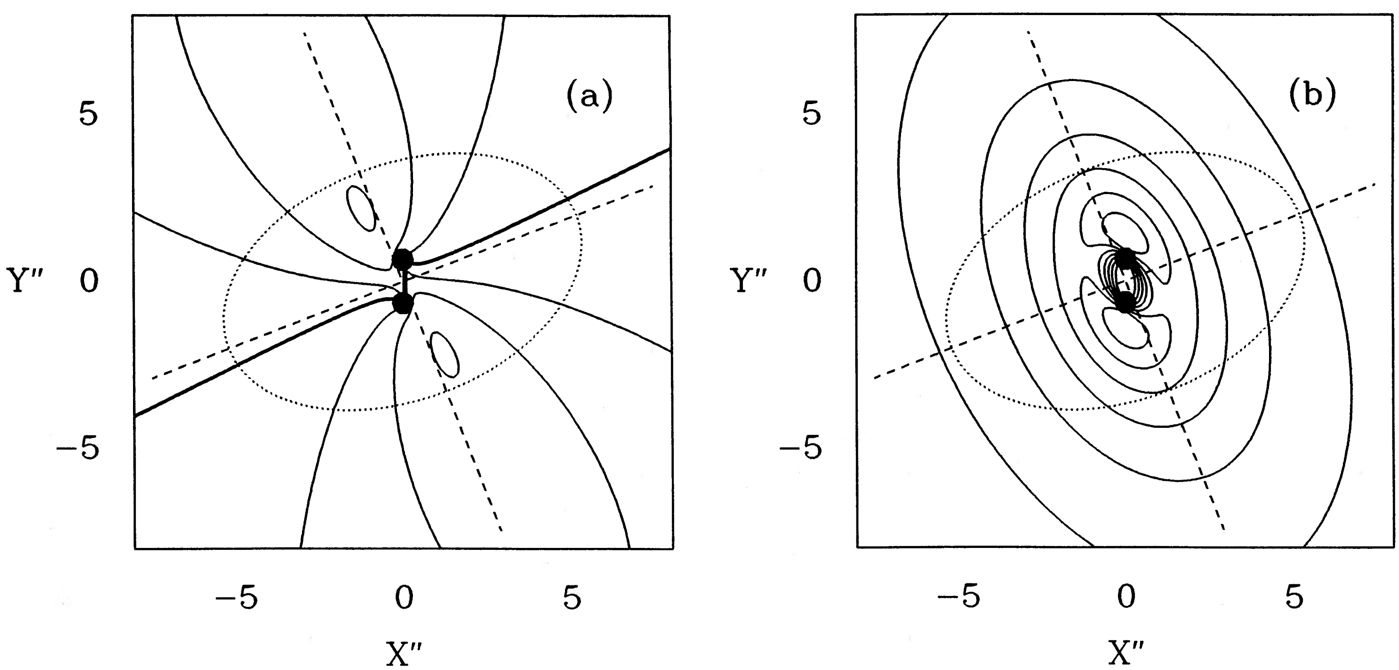

FIG. 7.—(*a*) Projected velocity field of gas on elliptic closed orbits in the (y, z)-plane of the perfect ellipsoid with axis ratios 1:0.625:0.5, for viewing angles $\vartheta = 60°$ and $\varphi = 45°$. The contours of constant radial velocity are drawn at linear intervals. The thick curve is the zero velocity curve. The filled circles denote the foci. The principal axes of the projected stellar density distribution are indicated by the dashed lines. The dotted ellipse is a contour of constant projected stellar density. (*b*) Projected surface density of the gas for the same model.

The two zero-velocity points are located at

$$x'' = \pm \frac{k^2 \sin\varphi \cos\varphi \sin\vartheta}{\sqrt{k^2(\cos^2\vartheta + \sin^2\varphi \sin^2\vartheta) + (\gamma - \beta)\cos^2\vartheta}} ,$$

$$y'' = \pm \frac{(k^2 \cos^2\varphi + \gamma - \beta)\sin\vartheta \cos\vartheta}{\sqrt{k^2(\cos^2\vartheta + \sin^2\varphi \sin^2\vartheta) + (\gamma - \beta)\cos^2\vartheta}} , \tag{3.31}$$

so that they have position angles Θ_v and $\Theta_v + \pi$ with respect to the y''-axis, given by

$$\tan\Theta_v = -\frac{k^2 \sin\varphi \cos\varphi}{(\gamma - \beta + k^2 \cos^2\varphi)\cos\vartheta} . \tag{3.32}$$

In terms of r_v and Θ_v, expression (3.26) for the zero-velocity curve can be written as

$$r_v^2 \sin 2(\Theta_x - \Theta_v) = (\gamma - \beta)\sin^2\vartheta \sin 2\Theta_x , \tag{3.33}$$

where Θ_x, the position angle of the projected x-axis, was defined in equation (3.3).

Just as for the gas ellipse in the (x, y)-plane, the tangent of the projected ellipse at the zero velocity point is perpendicular to the projection of the normal to the plane, i.e., the projection of the x-axis. As a result, we have the following relation between the angles Θ_{gas}, Θ_v, and Θ_x:

$$\tan(\Theta_{gas} - \Theta_x) = \frac{k_1^2}{k_2^2}\tan(\Theta_{gas} - \Theta_v) . \tag{3.34}$$

The two other points of intersection of the hyperbola (3.26a) and the projected ellipse are given by

$$x'' = \mp \frac{k^2 \cos\varphi \cos\vartheta}{\sqrt{k^2(\cos^2\vartheta + \sin^2\varphi \sin^2\vartheta) + (\gamma - \beta)\sin^2\varphi \sin^2\vartheta}} ,$$

$$y'' = \pm \frac{[k^2 + (\gamma - \beta)\sin^2\vartheta]\sin\varphi}{\sqrt{k^2(\cos^2\vartheta + \sin^2\varphi \sin^2\vartheta) + (\gamma - \beta)\sin^2\varphi \sin^2\vartheta}} . \tag{3.35}$$

At these points the tangent to the ellipse is parallel to the projected x-axis.

d) Projection of the Density Distribution

Franx (1988) has proved that the density of any triaxial model with a Stäckel potential projects to a symmetric distribution. He showed that the projected density distribution has a special form in elliptic coordinates (λ', μ'), which are the solution for τ of

$$\frac{x'^2}{\tau - \mu_a} + \frac{y'^2}{\tau - \nu_a} = 1 , \tag{3.36}$$

with $\nu_a \le \mu' \le \mu_a \le \lambda'$; (μ_a, ν_a) are equal to the asymptotic ellipsoidal coordinates of the line of sight, and (x', y') are Cartesian coordinates aligned with the symmetry axes. Specifically (see also Appendix A of Z85),

$$\nu_a = \tfrac{1}{2}(d_1 - \Delta'^2) , \qquad \mu_a = \tfrac{1}{2}(d_1 + \Delta'^2) , \tag{3.37}$$

with

$$d_1 = -2\gamma + (\gamma - \alpha)(\sin^2\varphi + \cos^2\varphi \cos^2\vartheta) + (\gamma - \beta)(\cos^2\varphi + \sin^2\varphi \cos^2\vartheta) ,$$

$$\Delta'^4 = [(\gamma - \alpha)(\sin^2\varphi - \cos^2\varphi \cos^2\vartheta) + (\gamma - \beta)(\cos^2\varphi - \sin^2\varphi \cos^2\vartheta)]^2 + 4(\beta - \alpha)^2 \sin^2\varphi \cos^2\varphi \cos^2\vartheta . \tag{3.38}$$

Given μ_a and ν_a, we can find the corresponding angles ϑ and φ by means of the relations

$$\cos^2\vartheta = \frac{(\mu_a + \gamma)(\nu_a + \gamma)}{(\gamma - \alpha)(\gamma - \beta)} , \qquad \tan^2\varphi = \frac{(\mu_a + \beta)(\nu_a + \beta)(\gamma - \alpha)}{(\mu_a + \alpha)(\nu_a + \alpha)(\beta - \gamma)} . \tag{3.39}$$

Franx (1988) furthermore shows that the x'-axis has a position angle Θ_* given by

$$\tan 2\Theta_* = \frac{2(\beta - \alpha)\sin\varphi \cos\varphi \cos\vartheta}{(\gamma - \alpha)(\sin^2\varphi - \cos^2\varphi \cos^2\vartheta) + (\gamma - \beta)(\cos^2\varphi - \sin^2\varphi \cos^2\vartheta)} , \tag{3.40}$$

where

$$(\beta - \alpha)\sin 2\Theta_* \sin 2\varphi \cos\vartheta \le 0 \quad \text{and} \quad -\frac{\pi}{2} < \Theta_* \le \frac{\pi}{2} . \tag{3.41}$$

An alternative expression for Θ_* is

$$\tan^2\Theta_* = -\frac{(\nu_a + \alpha)(\nu_a + \beta)(\mu_a + \gamma)}{(\mu_a + \alpha)(\mu_a + \beta)(\nu_a + \gamma)} . \tag{3.42}$$

It is evident from equation (3.40) that Θ_* *depends only on* $\gamma - \alpha$, $\gamma - \beta$, *and the viewing angles* ϑ *and* φ, *and hence is independent of the specific density distribution of the Stäckel model.* It should be noted that the above equations are valid for all α, β, and γ, also when these parameters do not satisfy the condition $\alpha \le \beta \le \gamma$.

The elliptic coordinate system (λ', μ') has its foci at $(x', y') = (0, \pm\Delta')$. Given a projected Stäckel model, it is possible to derive their location directly from the projected density distribution (see § IV*a*). It is straightforward to prove that these projected foci lie on the two branches of the zero-velocity hyperbolae (3.11) and (3.26) of the closed orbits of the (x, y)-plane and the (y, z)-plane. Since each of the branches of one hyperbola intersects the other hyperbola only once, the projected foci lie on the intersection of both hyperbolae, at $(x'', y'') = (\mp\Delta' \sin\Theta_*, \pm\Delta' \cos\Theta_*)$.

The symmetry axes of the projected density distribution are indicated in Figures 3, 5, and 7. For most Stäckel models, the x'-axis is the major axis. It is straightforward to calculate the position-angle difference $\Phi = \Theta_* - \Theta_{\rm gas}$ between a projected gas ring and the stellar distribution. In Figure 8 we present contours of constant Φ on the unit sphere of projection directions for the gas ring that we also used in Figure 6, with $l_1 = 1.85$ and $l_2 = 1.0$. The mass model is the same perfect ellipsoid as used there. The case where the gas ring is in the plane perpendicular to the short axis of the model is shown in Figure 8*a*. The other possibility, with the gas ring in the plane perpendicular to the long axis of the model, is shown in Figure 8*b*. Clearly, substantial misalignments between the apparent major axis of the stellar light and the apparent major axis of the gas ring are possible.

It is useful to give the explicit forms of the above results for the special case of the perfect ellipsoid, which is the unique Stäckel model in which the density is stratified exactly on similar concentric ellipsoids (de Zeeuw and Lynden-Bell 1985). The density distribution is given by

$$\rho(x, y, z) = \frac{\rho_0}{(1 + m^2)^2}, \tag{3.43}$$

where

$$m^2 = \frac{x^2}{a^2} + \frac{y^2}{b^2} + \frac{z^2}{c^2}, \tag{3.44}$$

and ρ_0 is the central density. The potential is of Stäckel form in the ellipsoidal coordinates (λ, μ, ν) defined by $\alpha = -a^2$, $\beta = -b^2$, $\gamma = -c^2$. In these coordinates the density distribution can be written as

$$\rho(\lambda, \mu, \nu) = \rho_0\left(\frac{\alpha\beta\gamma}{\lambda\mu\nu}\right)^2. \tag{3.45}$$

The projected surface density $\Sigma(x', y')$ is given by

$$\Sigma(x', y') = \frac{abc}{a'b'}\frac{\pi}{2}\frac{\rho_0}{(1 + m'^2)^{3/2}}, \tag{3.46}$$

with

$$m'^2 = \frac{x'^2}{a'^2} + \frac{y'^2}{b'^2}. \tag{3.47}$$

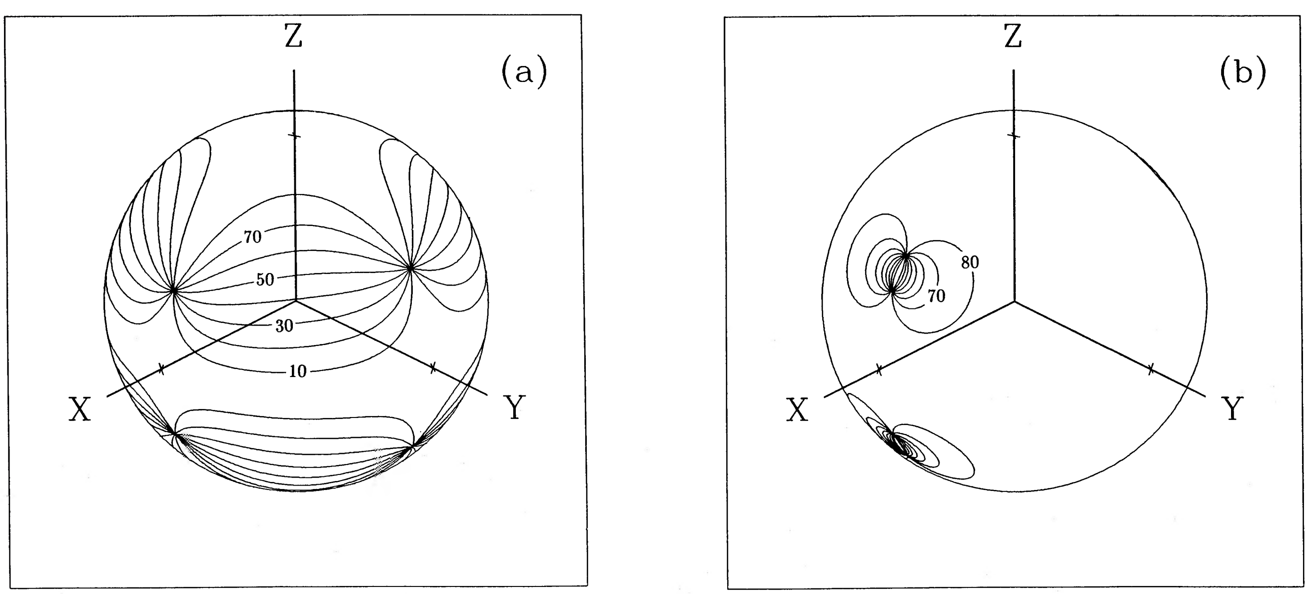

FIG. 8.—Position-angle difference $\Phi = \Theta_* - \Theta_{\rm gas}$ for a gas ring in a perfect ellipsoid with axis ratios 1:0.625:0.5. Contours of constant Φ are drawn at intervals of 10° on the unit sphere of projection directions. (*a*) Gas ellipse in the (x, y)-plane with axis ratio 1.85:1. (*b*) Gas ellipse in the (y, z)-plane with axis ratio 1.25:1.

In terms of (λ', μ') we have

$$\Sigma(\lambda', \mu') = \frac{\pi abc\rho_0}{2a'b'}\left(\frac{\mu_a \nu_a}{\lambda'\mu'}\right)^{3/2} . \tag{3.48}$$

The axis lengths a', b' are related to the asymptotic coordinates (μ_a, ν_a) by

$$a'^2 = \mu_a, \qquad b'^2 = \nu_a. \tag{3.49}$$

The axis ratio $q = b'/a'$ of the projected distribution satisfies the constraint $c/a \le q \le 1$. All values within this range are possible. Note that we have $\Delta' = a'(1 - q^2)^{1/2}$. Equation (3.40) for the tangent of $2\Theta_*$ reduces to the well-known expression for ellipsoidally stratified mass models (Kondrat'ev and Ozernoy 1979; Binney 1985).

IV. DEPROJECTION OF STARS AND GAS

We now consider a projected triaxial Stäckel model containing a gas ring or disk, and discuss in detail how the observed properties can be used to constrain the intrinsic properties of the model. Where the potential is needed, we assume that the mass-to-light ratio M/L of the stellar population is constant, so that the projected surface brightness distribution is proportional to the projected surface density distribution. Note that not all the results depend on this assumption. First we consider the deprojection of the stellar light. Then we include the morphology and kinematics of first one and then two gas rings. Finally, we discuss the case of an extended disk of gas, and we delineate the results that are valid also for nonseparable models.

a) Deprojection of Stellar Light

Let $\Sigma(x'', y'')$ be the surface density distribution of a projected Stäckel model. Determination of the symmetry axis of Σ gives $\hat{\Theta}_*$, the position angle of the apparent major axis with respect to north, and hence defines the coordinate system (x', y') in which $\Sigma(x', y')$ is symmetric. The surface density Σ at a general point (x', y') is fixed completely by specification of the surface density profile $\Sigma(0, y')$ along the apparent minor axis, and the value of Δ', which defines the elliptic coordinate system (λ', μ') of § III*d* (see eqs. [61]–[63] of Franx 1988). In particular, given $\Sigma(0, y')$, the observed ellipticity profile follows from Δ'. Thus, the observed surface density distribution provides us with two parameters, $\hat{\Theta}_*$ and Δ', and a function of one variable, $\Sigma(0, y')$.

In order to obtain the intrinsic shape of the triaxial model, we need to determine the three viewing angles ϑ, φ, and χ, the two parameters $\gamma - \alpha$ and $\gamma - \beta$ that define the ellipsoidal coordinates (λ, μ, ν), and the density profile $\rho(0, 0, z)$. The condition that the potential of the model is of Stäckel form then gives the density $\rho(x, y, z)$ at a general point through Kuzmin's formula (Kuzmin 1973; de Zeeuw 1985*b*). It is evident that knowledge of $\hat{\Theta}_*$, Δ', and $\Sigma(0, y')$ is not sufficient to determine all these quantities, and hence the deprojection of just the stellar surface density distribution is not unique.

For subsequent use, it is of interest to consider the case where we know the viewing angles ϑ, φ, and χ. This allows us to derive $\gamma - \alpha$ and $\gamma - \beta$ from the observed values of Δ' and $\hat{\Theta}_*$. By combining equations (3.38), (3.40), and (3.41) we find

$$\sin[2(\hat{\Theta}_* - \chi)] = -\frac{(\beta - \alpha)h_3}{\Delta'^2}, \qquad \cos[2(\hat{\Theta}_* - \chi)] = -\frac{(\gamma - \alpha)h_1 + (\gamma - \beta)h_2}{\Delta'^2}, \tag{4.1}$$

where we have written

$$h_1 = \sin^2\varphi - \cos^2\varphi\cos^2\vartheta, \qquad h_2 = \cos^2\varphi - \sin^2\varphi\cos^2\vartheta, \qquad h_3 = 2\sin\varphi\cos\varphi\cos\vartheta, \tag{4.2}$$

so that $h_1 + h_2 = \sin^2\vartheta$. Since h_1, h_2, and h_3 are assumed to be known, and Δ' is measured, we find

$$\begin{aligned} \gamma - \alpha &= -\Delta'^2 \frac{h_3\cos[2(\hat{\Theta}_* - \chi)] + h_2\sin[2(\hat{\Theta}_* - \chi)]}{h_3\sin^2\vartheta}, \\ \gamma - \beta &= -\Delta'^2 \frac{h_3\cos[2(\hat{\Theta}_* - \chi)] - h_1\sin[2(\hat{\Theta}_* - \chi)]}{h_3\sin^2\vartheta}, \\ \beta - \alpha &= -\Delta'^2 \frac{\sin[2(\hat{\Theta}_* - \chi)]}{h_3}. \end{aligned} \tag{4.3}$$

If we require the x-axis to be the long axis of the model, and the z-axis the short axis, then the only physical solutions for $\gamma - \alpha$ and $\gamma - \beta$ are those for which $\alpha \le \beta \le \gamma$. The above expressions are still valid when this last inequality is not satisfied. In that case, the foci will lie on different axes, and the model will be elongated differently.

Although a choice of the viewing angles ϑ, φ, and χ allows a determination of the ellipsoidal coordinate system in which the potential of the model is of Stäckel form, in general the function $\Sigma(0, y')$ cannot be used to determine $\rho(0, 0, z)$, and hence $\rho(x, y, z)$, uniquely (Franx 1988). Thus, in these cases even specification of the direction of viewing does not make the deprojection of a Stäckel model unique.

In the special case where the Stäckel model is a perfect ellipsoid (3.43), the value of Δ' is equal to $(a'^2 - b'^2)^{1/2}$ and hence follows immediately from the observed axes a', b'. Equation (4.3) then gives $a^2 - c^2$ and $b^2 - c^2$ for assumed values of ϑ, φ, and χ. The axis c follows from equations (3.49), (3.37), and (3.38), so that all axis lengths and axis ratios are fixed. For this special case the deprojection is therefore unique once the viewing angles have been specified. This result is valid not only for the perfect ellipsoid but also for all mass models in which the density is stratified exactly on similar, concentric, ellipsoids (Stark 1977). We remark that for these models we may also derive b/a and c/a from the observed value of b'/a' and Θ_*, if both ϑ and φ are known. The relevant equations are derived in Appendix A.

b) *One Gas Ring*

In §§ III*b*(ii) and III*c*(ii) we considered the projection of a ring of cold gas in a Stäckel potential. Here we discuss the deprojection of such a gas ring. We again assume a constant M/L ratio for the stars. In the first part, we use only those projected properties which are determined by the geometry of the coordinate system and are independent of the form of the function $G(\tau)$. In the second part, we include the radial mass distribution to derive further constraints on the viewing angles.

i) *Geometric Properties*

The morphology of the projected gas ring is fully determined by the intrinsic ellipsoidal coordinates and the viewing angles. The same holds for the point at which the radial velocity is zero, and also for the foci of the projected density distribution. The observational parameters which can be measured easily are l_1, l_2, $\hat{\Theta}_{\rm gas}$, r_v, $\hat{\Theta}_v$, Δ', and $\hat{\Theta}_*$. Since the zero-velocity points lie on the ellipse defined by l_2, l_2, and $\hat{\Theta}_{\rm gas}$, it follows that r_v and $\hat{\Theta}_v$ are not independent. Furthermore, the foci of the projected gas ring, the foci of the (λ', μ')-coordinates and the zero-velocity points of the ring all lie on the same hyperbola in the plane of projection. This hyperbola has orthogonal asymptotes, and therefore it is specified by two points. As a result, the hyperbola can be drawn if the apparent shape of the gas ring is measured, and if the zero-velocity points are determined. The focus Δ' is then completely defined by the position angle $\hat{\Theta}_*$, since it lies on the intersection of the minor axis of the projected stellar distribution and the zero-velocity hyperbola. Hence, of the seven observational parameters, only five can be used to constrain the intrinsic shape and orientation, since two of the parameters can be derived from the others without explicit deprojection. This redundancy allows us to check independently of the projection angles whether our underlying assumptions are valid. The six intrinsic parameters are the projection angles ϑ, φ, and χ, the quantities $\gamma - \alpha$ and $\gamma - \beta$ that define the ellipsoidal coordinates, and the intrinsic minor-axis length l of the gas ellipse, given by $l^2 = \lambda_0 + \alpha$. The deprojection is not fully determined by the five observational parameters, and one degree of freedom will remain.

In practice, the deprojection may be done as follows. We define the plane in which the gas ring lies to be the (x, y)-plane. The z-axis perpendicular to this plane is not necessarily the short axis of the density distribution. We have seen in § III*b*(ii) that the tangent of the projected ellipse at the zero-velocity point is perpendicular to the projected z-axis, i.e., the y''-axis. Hence the direction of the y''-axis can be determined immediately, so that χ follows. We then choose ϑ as our free parameter. For each value of ϑ we determine φ, l, and $\beta - \alpha$ from the properties of the projected gas ring. The parameter $\gamma - \beta$ can then be found from the observed value of Δ', which follows from the projected surface density distribution. Below we give the relevant equations.

First use the observed axis ratio l_1/l_2 of the ellipse and the difference between the position angle $\hat{\Theta}_{\rm gas}$ of the apparent major axis and that of the zero-velocity point, $\hat{\Theta}_v$, to determine χ, by means of the relation

$$\tan(\hat{\Theta}_{\rm gas} - \chi) = \frac{l_1^2}{l_2^2} \tan(\hat{\Theta}_{\rm gas} - \hat{\Theta}_v) , \tag{4.4}$$

which follows immediately from equation (3.21). Then use the distance r_v of the zero-velocity point to the center, and the semiaxes l_1 and l_2 of the ellipse to calculate the auxiliary quantities

$$e_1 = r_v^2 \sin[2(\hat{\Theta}_v - \chi)] , \qquad e_2 = -\frac{e_1}{\tan[2(\hat{\Theta}_{\rm gas} - \chi)]} , \qquad e_3 = l_1^2 + l_2^2 . \tag{4.5}$$

Since we have (cf. eqs. [3.13], [3.14], and [3.18])

$$\begin{aligned} e_1 &= 2(\beta - \alpha) \sin\varphi \cos\varphi \cos\vartheta , \\ e_2 &= l^2 \sin^2\vartheta + (\beta - \alpha)(\cos^2\varphi - \sin^2\varphi \cos^2\vartheta) , \\ e_3 &= l^2(1 + \cos^2\vartheta) + (\beta - \alpha)(\cos^2\varphi + \sin^2\varphi \cos^2\vartheta) , \end{aligned} \tag{4.6}$$

it is straightforward to show that

$$\tan 2\varphi = \frac{2e_1 \cos\vartheta}{e_2(1 + \cos^2\vartheta) - e_3 \sin^2\vartheta} , \qquad e_1 \sin 2\varphi \cos\vartheta \geq 0 , \tag{4.7}$$

and

$$\beta - \alpha = \frac{e_1}{\sin 2\varphi \cos\vartheta} , \tag{4.8}$$

$$l^2 = \tfrac{1}{2}(e_2 + e_3) - \Delta^2 \cos^2\varphi . \tag{4.9}$$

Thus, for each assumed value of ϑ, we can calculate φ, l, and $\beta - \alpha$. The values of $\gamma - \alpha$ and $\gamma - \beta$ then follow from the known values of Δ' and $\hat{\Theta}_*$ via relations (4.3). All our solutions will satisfy $\beta - \alpha \geq 0$. Values of ϑ for which $\alpha \leq \beta \leq \gamma$ correspond to models that have the x-axis as the long axis and the z-axis as the short one. If $\gamma \leq \alpha \leq \beta$, then the z-axis is the long axis of the model, and the y-axis is the short axis. In case $\alpha \leq \gamma \leq \beta$, the x-axis is the long axis and the z-axis is the intermediate axis. Elliptic closed orbits around the intermediate axis are unstable (Heiligman and Schwarzschild 1979; Z85), and therefore such solutions are not permitted.

In the special case where the galaxy is oblate, the gas in the (x, y)-plane is on circular orbits, so that we have $\hat{\Theta}_v = \chi$ and

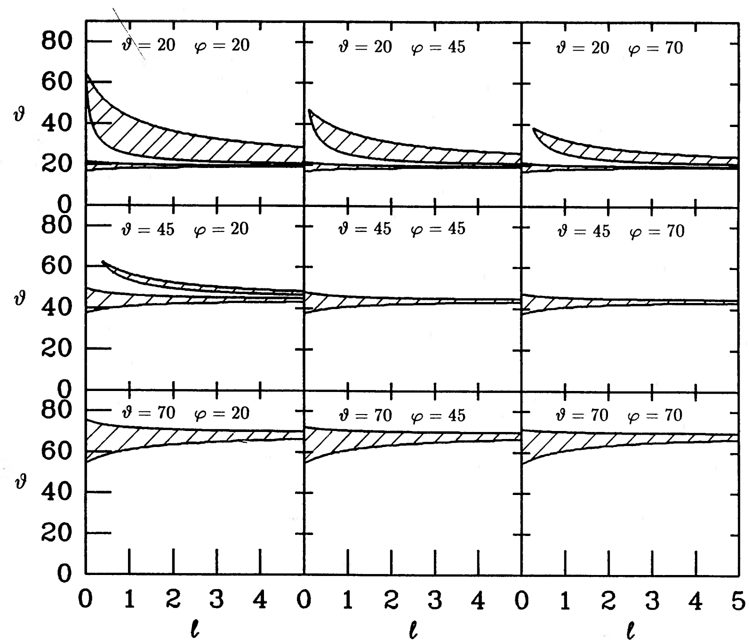

FIG. 9.—Deprojection of a gas ring in a perfect ellipsoid with semiaxes $a = 1.0$, $b = 0.625$, and $c = 0.5$. Each of the nine diagrams shows the allowed range of ϑ for possible deprojections of one specific projected model. The surface density of the stars, the geometry of the projected gas orbit, and the locations of the zero-velocity points have been used to find the possible deprojections of the projected model. For each value of the semiminor axis length l of the gas ellipse, the range of possible values of ϑ is indicated by the hatched area. The assumed values of the projection angles ϑ and φ of the original model are given in the top left-hand corner of each of the nine panels. Further details are given in the text.

$\hat{\Theta}_* = \hat{\Theta}_{\rm gas} = \chi + \pi/2$. We now find $l = l_1$, $\cos\vartheta = l_2/l_1$, $\beta = \alpha$, and $\gamma - \alpha = \Delta'^2/\sin^2\vartheta$, while φ is arbitrary. Thus, as is well known, in this case all parameters can be determined. In the limit $\gamma - \beta$, the model is prolate with the x-axis as the long axis. The orbits in the (x, y)-plane now are the elliptic orbits over the pole, and are marginally unstable. Therefore, it is unlikely that gas in equilibrium is on these orbits, so that this situation will not be encountered.

We have seen in § IV*a* that given φ, χ, $\gamma - \alpha$, and $\gamma - \beta$, and an assumed value for ϑ, the deprojection of the observed surface density distribution is generally still nonunique, and $\rho(0, 0, z)$ cannot be determined from $\Sigma(0, y')$. The assumption that the intrinsic density is that of a perfect ellipsoid fixes the deprojection of the surface density completely. The scale factors a' and b', which follow from the surface photometry, allow a direct determination of γ for a given ϑ, by equation (3.38). Since in this case we have $\alpha = -a^2$, $\beta = -b^2$, and $\gamma = -c^2$, the allowed values for ϑ are those for which the resulting values of α, β, and γ satisfy

$$\alpha \le \beta \le \gamma \le 0 \quad \text{or} \quad \gamma \le \alpha \le \beta \le 0 , \tag{4.10}$$

so that the gas lies in one of the two permissible planes.

As an illustration, we have projected a perfect ellipsoidal model with $a = 1$, $b = 0.625$, and $c = 0.5$ in a given direction, calculated the observed properties of a gas ring in the (x, y)-plane with minor-axis length l, and then used the above procedure to derive the associated intrinsic shape, for assumed values of ϑ. Figure 9 shows the range of values of ϑ that give physical solutions for the intrinsic shape as function of l, for nine different directions of viewing. It is evident from the figure that the observable properties always allow solutions where the gas is in the (x, y)-plane, as expected. In many cases solutions where the gas is in the (y, z)-plane are found also. In all cases the allowed range for ϑ shrinks to the correct value, i.e., the one assumed for the projection of the original model, as $l \to \infty$, in agreement with the fact that in this limit the orbits become circular, and hence their apparent flattening and the location of the zero-velocity point determine the direction of viewing completely. In Figure 10 we consider one particular case, and we plot the derived values of a, b, and c as a function of the assumed value of ϑ. Negative values for a, b, and c correspond to unphysical solutions for which either α, β, or γ is larger than zero. It can be seen that all three semiaxes are physical in a finite range of ϑ only. This range is divided into three parts, depending on whether the z-axis is the long, the intermediate, or the short axis of the model. The range of values of ϑ allowed by condition (4.10) is indicated. Although this range is not very large, the shape of the corresponding models varies from flat to oblate and from prolate to flat. When this is applied to elliptical galaxies, we can constrain the allowed range of ϑ further by requiring that the intrinsic axis ratios lie between 0.3 and 1.0 (Binney and de Vaucouleurs 1981).

ii) *Radial Velocities*

For each value of ϑ for which the combined deprojection of the elliptic gas ring and the stellar surface density as described above gives physical values for l, φ, χ, $\gamma - \alpha$, and $\gamma - \beta$, the observed radial velocities can be used to derive the intrinsic velocity variation along the orbit. Equation (3.7) gives the velocity field as a function of x, y, λ_0, μ, and v_μ. We transform x, y to x'', y'' with equation (3.5), and obtain

$$v_r(x'', y'') = -\frac{\sin\vartheta}{l\sqrt{l^2 + \beta - \alpha}} \left\{ [l^2 + (\beta - \alpha)\sin^2\varphi]x'' + \frac{(\beta - \alpha)\sin\varphi\cos\varphi}{\cos\vartheta} y'' \right\} \frac{v_\mu}{\sqrt{\lambda_0 - \mu}} . \tag{4.11}$$

Here $\lambda_0 - \mu = l^2 - (\mu + \alpha)$ can be expressed in terms of x'' and y'' by use of the relation $(\mu + \alpha) = -x^2(\beta - \alpha)/l^2$. The factor in braces in equation (4.11) vanishes at the two points of zero velocity, and attains its maximum value independently of the value of ϑ at the two other points of intersection of the hyperbola (3.11), given in equation (3.22). It should be noted, though, that the maximum values of v_r generally is not reached at these points, since $v_\mu(\lambda_0 - \mu)^{-1/2}$ also varies along the orbit.

The orbital velocity v_μ is smallest on the y-axis. This is due to the elliptical shape of the orbit, and is independent of the precise potential of the model. In principal this allows a determination of ϑ, since there is only one value for which v_μ as calculated by equation (4.11) has a minimum that coincides with the y-axis. In practice this may not be very easy, since ultraprecise measurements will be needed to determine the minimum of v_μ well. Even if all the velocities along the gas ring are measured, it remains difficult to constrain ϑ. To illustrate this, we consider again the perfect ellipsoid with axis lengths 0.5:0.625:1.0, with a gas ring in the (x, y)-plane at $l = 1.0$, so that the ring has an intrinsic axis ratio of 0.79, and we project it with viewing angles $\vartheta = 70°$ and $\varphi = 45°$. We then use the method of § IVb(i), and we determine all values of ϑ which would give a physical deprojection of the model. For these ϑ's we calculate the predicted observed radial velocities along the projected ellipse. The results are shown in Figure 11. It is evident that the allowed deprojections all give rather similar radial velocity profiles. The largest difference between the profiles is only 10% of the maximum observed radial velocity.

By the equation of continuity, the surface density of the gas is highest where the orbital velocity is smallest, i.e., on the y-axis. As a result, in principle we may also use the deprojected surface density of the gas ring to determine ϑ. This method may be difficult to use, as it is very hard to determine the surface density of a gas disk accurately.

Similar results may be obtained if the gas is in the (y, z)-plane, i.e., perpendicular to the long axis of the model. As we have seen in § IVb(ii), this case may be treated by allowing values of γ, β and α that satisfy $\gamma \le \alpha \le \beta$. If we need the expression for $v_r(x'', y'')$ for gas in this plane in the same coordinates also used for the (x, y)-plane, then we can apply the transformation described in § IIIc to equation (4.11). This gives

$$v_r(x'', y'') = \frac{1}{k\sqrt{k^2 + \gamma - \beta}} \left[(k^2 \cos^2 \varphi + \gamma - \beta) x'' \frac{\cos \vartheta}{\cos \varphi} - k^2 y'' \sin \varphi \right] \frac{v_\nu}{\sqrt{\kappa_0 - \nu}}, \tag{4.12}$$

where $\kappa_0 - \nu = k^2 - (\nu + \beta)$, and $\nu + \beta = -y^2(\gamma - \beta)/k^2$.

c) *Two Gas Rings*

In the previous section we have shown that in the most favorable case, the morphology and kinematics of one elliptic gas ring in a triaxial model allow the derivation of the viewing angles ϑ, φ, and χ, the intrinsic minor-axis length l of the ellipse, and the parameter $\beta - \alpha$. If another ring is present in the same plane, the viewing angles will be better constrained from observations of both rings. In principle, an accurate determination of the apparent shape and orientation of two rings in one plane suffices to determine the viewing angles. As the foci of the two projected ellipses lie on the zero-velocity hyperbola, the hyperbola is completely determined, and hence we know the direction of the projected z-axis. Furthermore, we can deproject the two ellipses for all values of ϑ. Only solutions for which the two projected ellipses have the same foci are valid. Observations of the velocities along the two rings will constrain the solutions better. It is clear that although the occurrence of two gas rings in the same plane helps us with the deprojection, it will not give us extra information about the potential or density outside the plane. Hence, as in § IVb, again the full three-dimensional coordinate system can be determined only by use of the stellar surface brightness distribution and the assumption that M/L is constant.

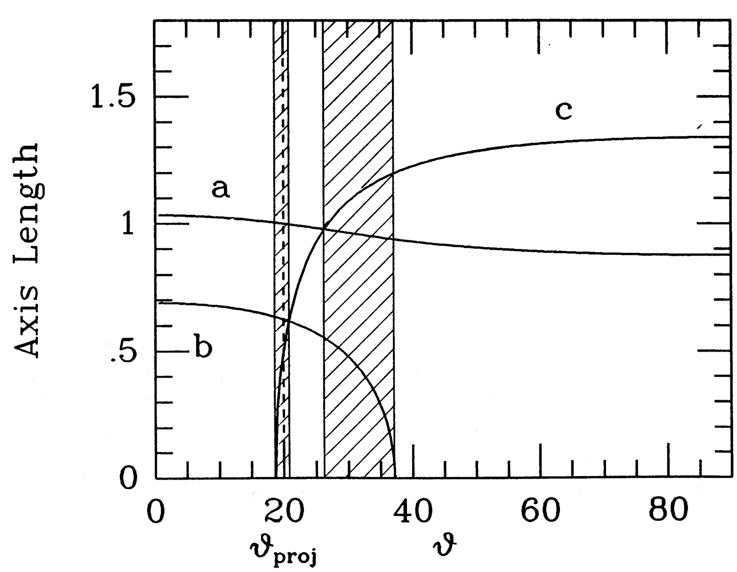

FIG. 10.—Deprojection of a gas ring in a perfect ellipsoid. The values of a, b, and c are shown as a function of ϑ for the case of a projected perfect ellipsoid with axis ratios 0.5:0.625:1.0 with projection angles $\vartheta = 20°$ and $\varphi = 45°$. The hatched areas indicate the allowed ranges of ϑ.

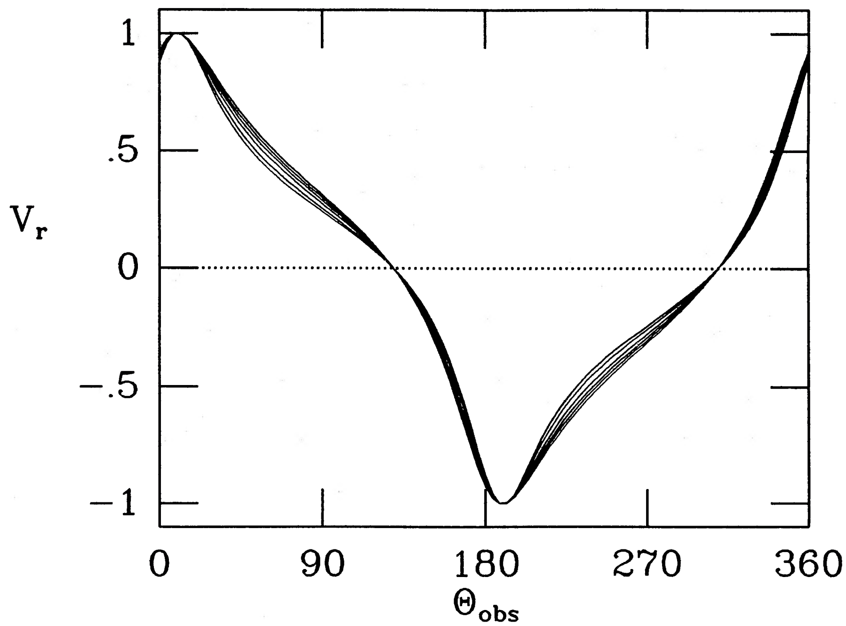

FIG. 11.—Variation of the radial velocity along the projected gas ring for the deprojections at the possible values of the angle ϑ. The original model is a perfect ellipsoid with axis ratios 0.5:0.625:1 projected at angles $\vartheta = 70°$ and $\varphi = 45°$.

Evidently, if we want to determine the intrinsic shape and the potential independently of the stellar surface brightness distribution, we need further information. This can be provided if the galaxy has two intrinsically perpendicular gas rings, one in each of the two preferred planes. This situation might apply to a disk galaxy with a triaxial halo and a polar ring, or to an elliptical galaxy with two gas rings. It turns out that in this case not only the orientation but also the complete three-dimensional (λ, μ, ν)-coordinate system can be determined. The geometric properties of the projected rings, and the location of the zero-velocity points on both rings, suffice to fix all three viewing angles, as well as $\gamma - \alpha$ and $\gamma - \beta$. Any other observed property is redundant, in the sense that it is not needed if the previously mentioned parameters are measured with infinite accuracy. In practice, extra information will constrain the solutions better.

Figure 12 shows a typical case. Since we do not know which of the two ellipses lies in the plane perpendicular to the short axis and which one in the plane perpendicular to the long axis, we arbitrarily choose ellipse 1 to lie in the (x, y)-plane and ellipse 2 to be in the (y, z)-plane. This ambiguity means that in the subsequent analysis we must allow solutions where the x-axis is either the long or the short axis, with the opposite for the z-axis, so that the y-axis is always the intermediate axis. If we assume that the zero-velocity points on both ellipses are known, then the tangents to the ellipses at these points give the angles $\hat{\Theta}_z = \chi$ and $\hat{\Theta}_x$ of the projected z- and x-axes via equations (3.21) and (3.34), respectively. The tangent to ellipse 1 at the point of intersection with the projected x-axis is parallel to the projected y-axis, and, similarly, the tangent to ellipse 2 at the intersection with the projected z-axis is parallel to the y-axis. Thus $\hat{\Theta}_y$ can be determined from either one of the relations

$$\tan(\hat{\Theta}_y - \hat{\Theta}_{\mathrm{gas},1}) = -\frac{l_2^2}{l_1^2 \tan(\hat{\Theta}_x - \hat{\Theta}_{\mathrm{gas},1}},$$

$$\tan(\hat{\Theta}_y - \hat{\Theta}_{\mathrm{gas},2}) = -\frac{k_2^2}{k_1^2 \tan(\chi - \hat{\Theta}_{\mathrm{gas},2})}. \tag{4.13}$$

The projection angles ϑ and φ then are derived from χ, $\hat{\Theta}_x$, and $\hat{\Theta}_y$ by

$$\cos\vartheta = -\frac{\tan\varphi}{\tan(\hat{\Theta}_x - \chi)}, \qquad \tan^2\varphi = -\frac{\tan(\hat{\Theta}_x - \chi)}{\tan(\hat{\Theta}_y - \chi)}. \tag{4.14}$$

The parameters $\beta - \alpha$ and $\gamma - \beta$ now follow immediately from the location of the zero-velocity points, via equations (4.6), (4.9), and (3.33). Also, the length scales l and k of the two ellipses can be calculated from the observed axis length l_1, l_2, k_1, and k_2 by means of equations (3.13) and (3.28). The zero-velocity hyperbolae are now fixed, since we know their asymptotes and the location of the zero-velocity points and the foci of the gas ellipses. The points of intersection of the two hyperbolae then give the value of Δ' and the direction of the apparent symmetry axis of the model. Note that *this can be derived without making any use of the projected surface brightness distribution.* Furthermore, we may use the observed radial velocities to constrain the radial behavior of the potential and the associated density. This will be considered in § V.

d) *Gas Disk*

We now consider the case of an extended gas disk in the (x, y)-plane of the model. Under some circumstances, this situation is very similar to the one of a single gas ring, discussed in § IV*b*. If the disk has a well-defined elliptic edge, the analysis of § IV*b* can be

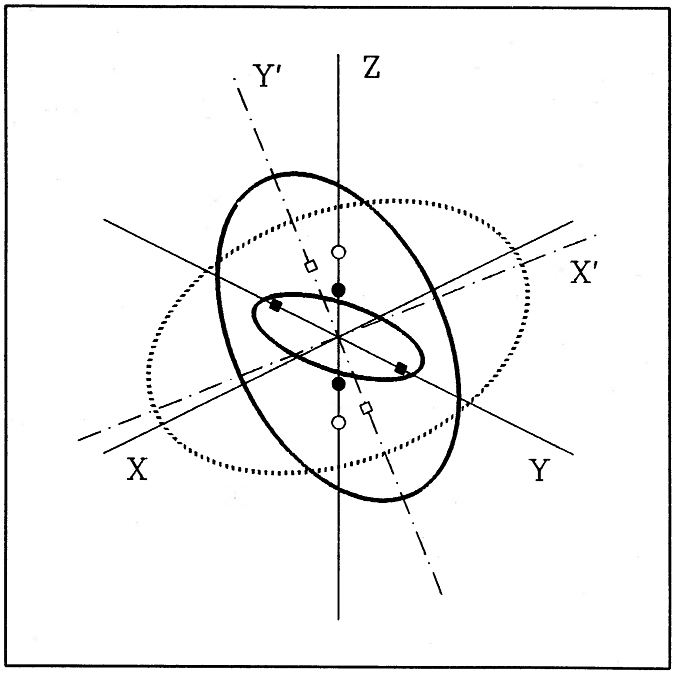

FIG. 12.—Two projected gas rings, one in each of the two preferred planes, in a perfect ellipsoid with $a = 1.0$, $b = 0.625$, and $c = 0.5$. The projection angles are $\vartheta = 60°$ and $\varphi = 45°$. The solid lines are the projected principal axes of the model. The foci on the principal axes are indicated by squares and filled and open circles. The x'- and y'-axes, which are the principal axes of the projected stellar density distribution, are indicated by the dash-dot lines. The open squares denote the associated foci. The dotted ellipse is a contour of constant projected density.

applied, as long as we read disk edge instead of gas ring. In particular, we may derive φ, χ, $\gamma - \alpha$, and $\gamma - \beta$ for each assumed value of ϑ, using the zero-velocity points on the edge, its geometric properties, and the surface density distribution of the stars (assuming constant M/L). Radial velocity variations in the disk may be used to constrain ϑ further.

If the edge of the gas disk is observationally ill-determined, we may proceed as follows. The observed zero-velocity curve over the extent of the gas disk gives the hyperbola (3.11), so that the position angle of the projected z-axis follows, and χ is known. Any point on the zero-velocity curve now gives the same constraint (3.18) on the values of ϑ, φ, and $\beta - \alpha$, so that $\beta - \alpha$ is known once ϑ and φ have been derived. This can be done if the fluxes of the emitting gas are well measured over an extended range in radii—although not necessarily all the way out to the edge. For each assumed ϑ and φ we deproject the observed surface density of the gas, and we ask for the cases where the derived intrinsic surface density not only has two perpendicular axes of symmetry but also has its direction of highest density coincide with the y-axis. This will generally determine both ϑ and φ. The parameter $\gamma - \beta$ then follows from the observed surface density distribution of the stars, by means of equation (4.3). Note that only one of the two parameters Δ' and $\hat{\Theta}_*$ is independent, since the foci associated with the surface density of the stars lie on the zero-velocity hyperbola (3.11) as well (§ III*b*[ii]). Physical solutions have $\alpha \leq \beta \leq \gamma$ for gas in the plane perpendicular to the short axis, and $\gamma \leq \alpha \leq \beta$ for a disk in the plane perpendicular to the long axis. As discussed in §§ IV*a* and IV*b*, further progress may be made if the model is assumed to be stratified on similar ellipsoids.

An interesting special case is that of a triaxial bulge in a disk galaxy. If we assume that the short axis of the bulge coincides with the rotation axis of the disk, then the inclination angle ϑ follows from the apparent flattening of the disk (which is assumed to be circular), and χ is known also. The procedure outlined above then allows a derivation of the remaining viewing angle φ, and the parameters $\gamma - \alpha$ and $\gamma - \beta$ from the gas velocities, so that the axis ratios of the bulge can be deduced. This case was considered by Gerhard and Vietri (1987).

We conclude that kinematic and photometric observations of a disk of gas combined with the surface photometry of the stellar light, and the assumption of a constant M/L, in principle give complete information on the orientation of a galaxy with a Stäckel potential. In practice, observational errors may complicate the procedure. If we do not want to use the surface density of the gas, then it follows from the above that we can determine χ, $\gamma - \alpha$, and $\gamma - \beta$ for each assumed combination of ϑ and φ. An application of the method described here to the elliptical galaxy NGC 5077, which contains a gas disk along its apparent minor axis, is given by Bertola *et al.* (1989*a*).

e) *Nonseparable Models*

We now consider briefly which of the results of the preceding sections are specific to Stäckel models and which are generic for a larger class of models.

i) *Nonrotating Triaxial Models*

In a general, i.e., nonseparable, nonrotating triaxial model with a finite core radius, the properties of the simple closed orbits are qualitatively similar to those in a triaxial Stäckel model. These orbits are approximately elliptic, become more nearly circular at large radii, and at small radii reduce to an oscillation of finite amplitide along the y-axis or along the z-axis (Schwarzschild 1979; Heilgman and Schwarzschild 1979). As a result, the zero-velocity curve will be similar to the one we have derived here. In particular, it will have a straight part along the projected y- or z-axis in the center and will become indistinguishable from the projected z- or x-axis at large radii. The special property in the case of a Stäckel model is that the orbits are exactly confocal ellipses, and therefore the curved parts of the zero-velocity curve lie on a hyperbola. Since the hyperbola has orthogonal asymptotes, it is defined by two points, and since the foci of the projected density distribution also lie on the hyperbola, this special property causes loss of information. It seems likely that such loss of information will not occur for the general case of the deprojection of a gas ring in a potential which is not of Stäckel form, although the deviations from a hyperbola may not be too large. *Hence the deprojection may be better constrained in the general case.*

The actual deprojection can be done in a way that is analogous to the deprojection of a gas ring in a Stäckel potential. As usual, we assume that the gas ring is in the (x, y)-plane. The tangent to the gas ring at the zero-velocity point determines the projected direction of its rotation axis, i.e., the z-axis. Then the ring is deprojected for all values of ϑ and φ. For each ϑ, the value of φ follows from the requirement that the deprojected ring must be symmetric with respect to the x- and y-axes. If we assume that M/L is constant, and that the stellar density distribution is stratified on similar concentric ellipsoids, then for each ϑ the observed surface brightness distribution can be deprojected. In particular, the intrinsic axis ratios b/a and c/a follow from the observed axis ratio b'/a' and the position angle Θ_* of the apparent major axis by means of equations (A3) and (A8). Since the shape of the gas ring is related to the shape of the model via the equations of motion and Poisson's equation, we can determine the value of ϑ by comparing the shape of the deprojected gas with the simple closed orbits in the deprojected model. The value of ϑ which reproduces the correct orbital shape gives the solution for the viewing angles. In practice, the closed orbits in the deprojected galaxy will have to be calculated by numerical means, but this is no major hurdle.

A similar method can be applied to the deprojection of an extended gas disk in a general nonrotating galaxy. One of the viewing angles can be deduced from the asymptotic position angle of the zero-velocity curve at large radii, since this gives the direction of the projected long or short axis. An alternative method would be to use the fact that the observed streaming and density along a line perpendicular to the projection of the angular momentum vector associated with the gas motion are related by (cf. Tremaine and Weinberg 1985)

$$\int \Sigma_g v_r \, ds = 0 \,. \tag{4.15}$$

This is a consequence of the equation of continuity and the absence of figure rotation. Given the observed surface density of the gas and the radial velocity field, we can calculate the above line integral along different position angles. The angle for which the integral vanishes gives the direction perpendicular to that of the projected principal axis around which the gas rotates. The remaining two viewing angles can be found by deprojecting the gas density distribution for all possible combinations and using the constraint that the deprojected density must be symmetric with respect to the x- and the y-axis. In this way, only a finite set of solutions χ, ϑ, φ should remain. The projected surface density of the stars can then be used to determine the intrinsic shape of the model, as described above.

ii) *Figure Rotation*

If the figure of the triaxial galaxy is rotating, the structure of the simple closed orbits becomes more complicated, because of the Coriolis force (Heisler, Merritt, and Schwarzschild 1982; Magnenat 1982). If the rotation is around the short axis, then the closed orbits in the (x, y)-plane still resemble those of the nonrotating case, except that the orbits never become exactly linear at small radii but instead become highly elongated ellipses. We expect that outside a core radius, and for slowly rotating systems such as elliptical galaxies, the results for a gas ring derived in § IV*b* may still be applied. However, in this case we have to introduce an extra parameter ω, the angular velocity of the galaxy, and it remains to be seen how this will influence the analysis, and the solution space. The orbits that originally were in the (y, z)-plane tip out of this plane in the general case of figure rotation around the short axis. The tip angle depends on the amplitude and the figure rotation speed, so that an extended gas disk will be warped (van Albada, Kotanyi, and Schwarzschild 1982). In this situation the analysis will become significantly more complicated and almost certainly will require numerical orbit calculations.

V. DERIVATION OF POTENTIAL

Although it is reasonable to assume that M/L is constant in the inner regions of a galaxy, there is ample proof that spiral galaxies have massive dark halos (e.g., van Albada and Sancisi 1986), and it is generally assumed that the same is true for elliptical galaxies. We therefore relax the assumption that M/L is constant, so that the density profile cannot be deduced from the luminosity distribution. We assume that the aspect angles ϑ, φ, and χ and the parameters $\gamma - \alpha$ and $\gamma - \beta$ that define the fundamental ellipsoidal coordinate system are known, and we investigate in which circumstances the observed radial velocities may be used to determine the function $G(\tau)$, which defines the potential by equation (2.1). This then allows the derivation of the total density distribution that generates the potential—i.e., the sum of the luminous and the dark material—and hence gives information on the behavior of M/L as a function of radius, and on the intrinsic shape of the galaxy.

We have seen in § IV that in practice ϑ, φ, χ, $\gamma - \alpha$, and $\gamma - \beta$ can be determined only if we have observations of two intrinsically perpendicular rings or disks of gas. If only one disk of gas is observed, then $\gamma - \beta$ cannot be determined from observations of the disk. We may only determine $\gamma - \beta$ from the stellar surface photometry, assuming a constant M/L. In this case we can use the results of this section as a consistency check of the assumption of a constant M/L.

a) Elliptic Orbits in the (x, y)-Plane

The velocity v_μ along an elliptic closed orbit in the (x, y)-plane is related to $G(\tau)$ by equation (2.8), which can be written as

$$\frac{v_\mu^2(\lambda, \mu)}{\lambda - \mu} = -2 \frac{\partial}{\partial \lambda} \left\{ \frac{(\lambda + \alpha)[G(\lambda) - G(\mu)]}{\lambda - \mu} \right\} . \tag{5.1}$$

We have seen in § IV*b* that given ϑ, φ, χ, $\gamma - \alpha$, and $\gamma - \beta$, the observed radial velocities $v_r(x'', y'')$ can be used to calculate $v_\mu(x'', y'')(\lambda - \mu)^{-1/2}$. By means of equations (3.5), and the relations

$$x^2 = -\frac{(\lambda + \alpha)(\mu + \alpha)}{\beta - \alpha} , \qquad y^2 = \frac{(\lambda + \beta)(\mu + \beta)}{\beta - \alpha} , \tag{5.2}$$

this can be expressed as $v_\mu(\lambda, \mu)(\lambda - \mu)^{1/2}$. As a result, the left-hand side of equation (5.1) is known, and we can consider this equation as a first-order partial differential equation for the quantity in braces. Integration with respect to λ gives

$$V_S(x, y, 0) = -\frac{(\lambda + \alpha)G(\lambda) - (\mu + \alpha)G(\mu)}{\lambda - \mu} = -\frac{1}{2} \int_\lambda^\infty \frac{v_\mu^2(\sigma, \mu)}{\sigma - \mu} \, d\sigma . \tag{5.3}$$

Here we have determined the constant of integration by the usual requirement that $G(\lambda) \sim GM/\sqrt{\lambda} \to 0$ for $\lambda \to \infty$, so that for a model with finite total mass M the potential $V_S \sim -GM/r$ at large radii r (where G is the constant of gravitation). In particular, we have

$$G(\lambda) = \frac{1}{2} \int_\lambda^\infty \frac{v_\mu^2(\sigma, -\alpha)}{\sigma + \alpha} \, d\sigma , \qquad G(\mu) = \frac{1}{2} \int_{-\alpha}^\infty \frac{v_\mu^2(\sigma, \mu)}{\sigma - \mu} \, d\sigma . \tag{5.4}$$

As a result, if the orbital velocities are known along the elliptic closed orbits in the complete (x, y)-plane of the model, we can determine $G(\tau)$ for all values of $\tau \geq -\beta$, and so obtain the potential in the whole (x, y)-plane, but not outside it.

Since $V_S(x, y)$ is determined by $G(\tau)$, which is a function of one variable, one would expect that the potential would follow from the radial velocities along a suitable curve in the (x, y)-plane, covered by all values of λ and μ. Although it is not obvious from equation (5.3), this is indeed the case. The velocities $v_\mu(\lambda, -\alpha)$ along the y-axis beyond the foci at $|y| \geq \Delta$ obviously determine $G(\lambda)$ via equation (5.4). According to equation (2.8), we have

$$G(\mu) = G(\lambda) - (\lambda - \mu) \frac{v_\mu^2(\lambda, \mu) - v_\mu^2(\lambda, -\alpha)}{2(\mu + \alpha)} . \tag{5.5}$$

Thus, once $G(\lambda)$ has been derived, $G(\mu)$ follows immediately from the variation of v_μ^2 along an elliptic closed orbit of constant λ. Here any value of $\lambda > -\alpha$ may be taken. Evidently, in a Stäckel model, the "rotation curve" along the y-axis of the closed orbits in the (x, y)-plane, and the velocities along one elliptic ring, determine the whole potential $V_S(x, y)$.

If the orbital velocities are available only out to a finite radius λ_{max}, then we cannot integrate $v_\mu^2/(\sigma + \alpha)$ up to infinity, as required in equation (5.4). However, in this case we may choose the constant of integration such that $G(-\alpha) = 0$, so that the integral for $G(\lambda)$ runs between $-\alpha$ and λ. This changes V_S by a constant, which does not affect any derived properties, such as the density. $G(\mu)$ again follows from equation (5.5), applied along any orbit with $-\alpha \leq \lambda \leq \lambda_{max}$. In this case the potential V_S is therefore known inside the ellipse $\lambda = \lambda_{max}$ in the (x, y)-plane.

For $\beta = \alpha$ the ellipsoidal coordinates reduce to prolate spheroidal coordinates, and the corresponding models generally are oblate with the z-axis as the symmetry axis (ZPF). The elliptic closed orbits in the (x, y)-plane reduce to the circular orbits in the equatorial plane. In this limit v_μ is identical to the circular velocity v_c, and equation (5.1). reduces to

$$v_c^2 = -2(\lambda + \alpha)G'(\lambda) = \varpi \frac{\partial V_S}{\partial \varpi}(\varpi, 0) . \tag{5.6}$$

Here we have used the fact that in the oblate limit the potential $V_S(\varpi, 0)$ in the equatorial plane is equal to $-G(\lambda)$, with $\lambda + \alpha = \varpi^2 = x^2 + y^2$. Equation (5.6) can be integrated immediately. The same result is obtained by taking the limit $\beta = \alpha$ of our expression (5.4) for $G(\lambda)$. We therefore recover the well-known result that the rotation curve of an oblate axisymmetric galaxy determines the potential in the equatorial plane, but not outside it.

b) Elliptic Orbits in the (y, z)-Plane

For the elliptic closed orbits in the (y, z)-plane we can perform a similar analysis. We use the observed values of $v_r(x'', y'')$ in order to calculate $v_\nu(x''. y'')(\kappa - \nu)^{-1/2}$. With equation (3.24) and the relations

$$y^2 = -\frac{(\kappa + \beta)(\nu + \beta)}{\gamma - \beta} , \qquad z^2 = \frac{(\kappa + \gamma)(\nu + \gamma)}{\gamma - \beta} , \tag{5.7}$$

this can be expressed as $v_\nu(\kappa, \nu)(\kappa - \nu)^{-1/2}$. The relation (2.16) between v_ν and $G(\tau)$, with $\tau = \lambda, \mu, \nu$, can then be written as

$$\frac{v_\nu^2(\kappa, \nu)}{(\kappa - \nu)} = -2 \frac{\partial}{\partial \kappa} \left\{ \frac{(\kappa + \gamma)[G(\kappa) - G(\nu)]}{(\kappa - \nu)} \right\} . \tag{5.8}$$

This is a first-order partial differential equation for the quantity in braces, given $v_\nu^2/(\kappa - \nu)$. Integration with respect to κ gives

$$V_S(0, y, z) = -\frac{(\kappa + \gamma)G(\kappa) - (\nu + \gamma)G(\nu)}{\kappa - \nu} = -\frac{1}{2}\int_\kappa^\infty \frac{v_\nu^2(\sigma, \nu)}{\sigma - \nu}\, d\sigma . \tag{5.9}$$

The constant of integration has been determined in the usual way. We obtain for $G(\tau)$

$$G(\kappa) = \frac{1}{2}\int_\kappa^\infty \frac{v_\nu^2(\sigma, -\gamma)}{\sigma + \gamma}\, d\sigma , \qquad G(\nu) = \frac{1}{2}\int_{-\gamma}^\infty \frac{v_\nu^2(\sigma, \nu)}{\sigma - \nu}\, d\sigma , \tag{5.10}$$

where $\kappa = \lambda, \mu$. We may also write

$$G(\nu) = G(\kappa) - (\kappa - \nu)\,\frac{v_\nu^2(\kappa, \nu) - v_\nu^2(\kappa, -\gamma)}{2(\kappa + \gamma)} . \tag{5.11}$$

As a result, if the velocities are known along the elliptic closed orbits in the whole (y, z)-plane of the model, we can determine $G(\tau)$ for all values of $\tau \geq -\gamma$ by a simple integration, so that the full three-dimensional potential of the model is known. In this case the "rotation curve" along the z-axis beyond the foci at $z = \pm\Delta_1$ determines $G(\kappa)$, and the velocity variation along any ellipse of constant κ gives $G(\nu)$. If we know the orbital velocities only out to $\kappa = \lambda_{max}$, then the constant of integration in the derivation of equation (5.10) for $G(\kappa)$ should be chosen such that $G(-\beta) = 0$. The integral for $G(\kappa)$ then runs between $-\beta$ and κ, and the potential inside the whole ellipsoid $\lambda = \lambda_{max}$ can be found. However, if we have velocities along just one elliptic orbit, then only $G(\nu)$ can be found.

In the limit $\gamma = \beta$, so that $\nu = -\beta$, the ellipsoidal coordinates reduce to oblate spheroidal coordinates, and the associated models are generally prolate with the x-axis as symmetry axis. The elliptic closed orbits in the (y, z)-plane now become the circular orbits in the equatorial plane. The above expression for the potential in terms of the orbital, i.e., circular, velocity reduces to the one derived by de Zeeuw and Lynden-Bell (1988, eq. [9]). In this case the rotation curve determines the potential of the whole model.

c) Density Distribution

The density distribution that corresponds to a Stäckel potential V_S can be calculated by means of Kuzmin's formula (Kuzmin 1973; de Zeeuw 1985*b*; ZPF), which is given by

$$\rho(\lambda, \mu, \nu) = g_\lambda^2 \psi(\lambda) + g_\mu^2 \psi(\mu) + g_\nu^2 \psi(\nu) + 2g_\lambda g_\mu \frac{\Psi(\lambda) - \Psi(\mu)}{\lambda - \mu} + 2g_\mu g_\nu \frac{\Psi(\mu) - \Psi(\nu)}{\mu - \nu} + 2g_\nu g_\lambda \frac{\Psi(\nu) - \Psi(\lambda)}{\nu - \lambda} , \tag{5.12}$$

where

$$g_\lambda = \frac{(\lambda + \alpha)(\lambda + \beta)}{(\lambda - \mu)(\lambda - \nu)} , \qquad g_\mu = \frac{(\mu + \alpha)(\mu + \beta)}{(\mu - \nu)(\mu - \lambda)} , \qquad g_\nu = \frac{(\nu + \alpha)(\nu + \beta)}{(\nu - \lambda)(\nu - \mu)} , \tag{5.13}$$

so that $0 \leq g_\lambda, g_\mu, g_\nu \leq 1$ and $g_\lambda + g_\mu + g_\nu = 1$. Here $\psi(\tau) = \Psi'(\tau)$ is the density profile $\rho(0, 0, z)$ along the z-axis (with $z^2 = \tau + \gamma$), and $\Psi(\tau)$ is given by

$$2\pi G\Psi(\tau) = (\tau + \gamma)\left[-\frac{2(\tau + \gamma)}{\tau + \beta} G'(\tau) - \frac{(\tau + \beta)^2 + (\beta - \alpha)(\gamma - \beta)}{(\tau + \alpha)(\tau + \beta)^2} G(\tau) + \frac{\gamma - \beta}{\tau + \beta} G'(-\beta) + \frac{\gamma - \alpha}{(\beta - \alpha)(\tau + \alpha)} G(-\alpha) - \frac{(\gamma - \beta)(\tau + 2\beta - \alpha)}{(\beta - \alpha)(\tau + \beta)^2} G(-\beta)\right] . \tag{5.14}$$

Kuzmin's theorem guarantees that $\rho(\lambda, \mu, \nu)$ as given in equation (5.12) is nonnegative everywhere if and only if $\psi(\tau) \geq 0$ for all $\tau \geq -\gamma$, i.e., if and only if $\rho(0, 0, z) \geq 0$ for all z. If $G(\tau)$ is a smooth function so are $\Psi(\tau)$, $\psi(\tau)$, and $\rho(\lambda, \mu, \nu)$.

The results of §§ V*a* and V*b* show that if the (x, y)-plane of the model contains an extended disk of gas, we can find $G(\tau)$, and hence $\Psi(\tau)$ and $\psi(\tau)$, only for $-\beta \leq \tau \leq \lambda_{max}$. Here λ_{max} is determined by the maximum distance out to which we can measure velocities. It follows from equation (5.12) that therefore we obtain the density along the z-axis for $\Delta_1 \leq |z| \leq z_{max}$, but nowhere else. Still, a comparison with the deprojected surface brightness profile will give an indication of the radial behavior of M/L. However, if the gas is in an extended disk in the (y, z)-plane, then we can find $G(\tau)$ for $-\gamma \leq \tau \leq \lambda_{max}$, and hence we obtain the density everywhere inside the ellipsoid $\lambda = \lambda_{max}$. As a result, M/L can be determined everywhere within this volume.

d) Fitting

In order to calculate the density distribution that corresponds to a given observed velocity field, we need $G(\tau)$ and its first two derivatives. We have seen in the above that this requires one differentiation of the intrinsic radial velocities. In practice, this may have to be done by numerical differencing of noisy data, which generally will not give very accurate results. This can be avoided by fitting the observed radial velocities with the velocity field of a smooth triaxial model, for which the associated density distribution can be calculated analytically.

De Zeeuw and Lynden-Bell (1988) discuss a set of convenient prolate Stäckel models for which the rotation curve rises linearly in the center, and decreases as $1/r^{p-1}$ at large radii r, with $1 \leq p \leq \frac{3}{2}$. The function $G(\tau)$ that defines these models has a very simple form, and can be used to define a set of triaxial Stäckel models. It is given by

$$G(\tau) = \begin{cases} -\frac{1}{2}A^2 \ln(\tau + \beta + \tau_0)\,, & p = 1\,, \\ \dfrac{A^2}{2(p-1)} \dfrac{1}{(\tau + \beta + \tau_0)^{p-1}}\,, & p \neq 1\,, \end{cases} \tag{5.15}$$

where A, τ_0, and $1 \leq p < \frac{3}{2}$ are parameters. For $p = 1$ the corresponding potential V_S given in equation (2.1) diverges logarithmically at large radii. For $p \neq 1$ it falls off as $1/z^{2(p-1)}$. It follows that the associated triaxial density distributions have infinite total mass, except for $p = \frac{3}{2}$. For values of p larger than $\frac{3}{2}$ the corresponding density distribution becomes negative at a finite radius. The parameter τ_0 can be considered as a scale length or core radius. In order for $G(\tau)$ to be well defined, τ_0 must be chosen such that $\tau_0 > \gamma - \beta$.

Gas on the elliptic closed orbits in the (x, y)-plane of a model defined by the choice (5.15) has a velocity field given by equation (2.7), with

$$\frac{v_\mu^2}{A^2} = \begin{cases} \dfrac{\lambda + \alpha}{\lambda + \beta + \tau_0} - \dfrac{\mu + \alpha}{\mu - \lambda} \ln\left(\dfrac{\mu + \beta + \tau_0}{\lambda + \beta + \tau_0}\right), & p = 1\,, \\ \dfrac{\lambda + \alpha}{(\lambda + \beta + \tau_0)^p} + \dfrac{\mu + \alpha}{(p-1)(\mu - \lambda)} \left[\dfrac{1}{(\mu + \beta + \tau_0)^{p-1}} - \dfrac{1}{(\lambda + \beta + \tau_0)^{p-1}}\right], & p \neq 1\,. \end{cases} \tag{5.16}$$

The observed radial velocity follows from equation (3.7). It is evident that for $p = 1$ the resulting "rotation curves" will be asymptotically flat, with $v_\mu \to A$ at large radii. Application of transformation (2.14) gives the expression for v_ν^2 from which the intrinsic and observed velocities for gas in the (y, z)-plane can be derived.

The functions $\Psi(\tau)$ and $\psi(\tau)$ that define the whole density distribution via Kuzmin's formula can be calculated by means of equation (5.14). The resulting expressions are fairly lengthy and are given in Appendix B, together with their oblate limits (see also Statler 1988). The properties of these models are very similar to those discussed in some detail for the prolate limit by de Zeeuw and Lynden-Bell (1988). For each p, models of different central flattenings may be obtained by varying $(\gamma - \alpha)/\tau_0$ and $(\gamma - \beta)/\tau_0$. For $p = 1$ the surfaces of constant density are approximately ellipsoidal, with axis ratios that increase monotonically outward and with arbitrary central flattenings. For $p > 1$ not all values of $(\gamma - \alpha)/\tau_0$ and $(\gamma - \beta)/\tau_0$ will give density profiles that are nonnegative everywhere. In this case the ellipticity profiles are not monotonic (cf. Fig. 2 of de Zeeuw and Lynden-Bell 1988). Bertola *et al.* (1989*a*) have used these models to fit the observed kinematics of the gas disk in the E3 galaxy NGC 5077.

VI. CONCLUDING REMARKS

The main conclusion which follows from this work is that observations of gas rings or disks in triaxial elliptical galaxies may be used to constrain the orientation and intrinsic shape significantly, if it can be assumed that the gas moves along simple periodic orbits. We have analyzed the deprojection of a gas ring in a Stäckel potential in detail, and we have shown that the three-dimensional solution space of the viewing angles is restricted to a one-dimensional curve if the apparent shape of the gas ring and the point of zero radial velocity are well determined. If very high precision measurements of the radial velocities are available, the solution space may be constrained further. In the case of two gas rings in the same plane, the viewing angles may be obtained from just the apparent shapes of the rings. Measurements of two perpendicular rings provide complete information about the viewing angles and the fundamental three-dimensional ellipsoidal coordinate system. In this case the full potential, and hence also the density and the radial behavior of M/L, may be determined if the plane perpendicular to the long axis of the galaxy is filled with gas.

These results, although derived specifically for a Stäckel potential, are fairly general. Surprisingly enough, the deprojection from one single gas ring is probably somewhat better constrained if the galaxy does not have a Stäckel potential. In this case, the deprojection is done in a similar way, the only difference being that we now have to calculate the orbits by numerical means. If we relax the assumption that the potential is of Stäckel form, we generally cannot determine the full three-dimensional potential from observations of gas in the two symmetry planes. However, we can still derive the potential in the planes which are filled with gas.

The most useful candidates for an analysis as outlined here are galaxies with (multiple) gas disks or rings which are not exactly aligned with the apparent major or minor axis. One of the consequences of the assumption of a triaxial potential is that the radial velocity is not zero when the gas ring is observed along its minor axis. This follows immediately from the geometry of a noncircular orbit. We have also shown that the determination of the point where the radial velocity is zero, combined with accurate surface photometry of the ring, immediately gives the projected rotation axis of the ring.

One of the major problems in the use of gas rings or disks for the deprojection of the galaxy is that we cannot be sure that the gas moves along stable closed orbits. Our knowledge of the processes which determine the evolution of the gas is still small. A well-known case where the gas may not be in equilibrium, although the velocity field is regular, is Cen A (e.g., Tubbs 1980; Wilkinson *et al.* 1986; Bland, Taylor, and Atherton 1987). If a gas disk is sufficiently massive, self-gravity may play an important role in its evolution (Sparke 1986). In this case, the gas may be in equilibrium, while it is not moving along stable periodic orbits. Although we may still use a similar method to find the orientation and shape of the gas ring in this case, it will be more difficult to derive the viewing angles of the galaxy, and hence its intrinsic shape. For galaxies with two orthogonal gas rings or disks we have redundant information, so that we can test whether the gas disks indeed lie in the symmetry planes of the galaxy. The surface density of the gas should be used with caution, as it is often clumpy and difficult to measure. Another worry may be our limited understanding of processes which determine radial streaming of the gas, if any occurs. If such streaming is caused by a "pseudo"-viscosity due to interaction between clouds, then the radial streaming velocity may depend on the shapes of the orbits, and thereby on the shape of the potential. This would have the interesting consequence that elliptical galaxies with long-lived gas disks, i.e., the ones most likely to be observed, would have potentials of special shape in the plane in which the gas resides. Hence intrinsic shapes derived for such galaxies would not necessarily be typical for elliptical galaxies.

It is a pleasure to thank Elaine Sadler and Lars Hernquist for stimulating discussions. M. F. acknowledges the hospitality of the Institute for Advanced Study. This research was supported in part by an RCA Fellowship to T. de Z.

APPENDIX A

DERIVATION OF b/a AND c/a, GIVEN ϑ, φ, b'/a' AND Θ_*.

Consider a triaxial model in which the density can be written as

$$\rho = \rho(m^2)\,, \qquad \text{with} \qquad m^2 = \frac{x^2}{a^2} + \frac{y^2}{b^2} + \frac{z^2}{c^2}\,, \tag{A1}$$

so that the density is stratified on similar concentric ellipsoids. For any direction of viewing, the projected surface density is constant on similar ellipses (e.g., Stark 1977) and may be written as

$$\Sigma = \Sigma(m'^2)\,, \qquad \text{with} \qquad m'^2 = \frac{x'^2}{a'^2} + \frac{y'^2}{b'^2}\,, \tag{A2}$$

where (x', y') are Cartesian coordinates aligned with the principal axes of the projected density distribution. Define δ', δ_1, and δ_2 by

$$\delta_1 = \frac{b^2}{a^2} - \frac{c^2}{a^2}\,, \qquad \delta_2 = 1 - \frac{c^2}{a^2}\,, \qquad \delta' = 1 - \frac{b'^2}{a'^2}\,. \tag{A3}$$

We now show that, if we assume values for the projection angles ϑ and φ, then the values of δ_1 and δ_2 can be calculated explicitly from observed values of δ' and Θ_*.

First consider the perfect ellipsoid (3.43), which is of the form (A1). We apply the general results for Stäckel models described in §§ III*d* and IV*a* to this case by taking $\gamma = -c^2$, $\beta = -b^2$, and $\alpha = -a^2$ in the relevant expressions. Hence, according to equation (4.3) we have

$$a^2 - c^2 = -a'^2\delta' \frac{h_3 \cos 2\Theta_* + h_2 \sin 2\Theta_*}{h_3 \sin^2 \vartheta}\,,$$

$$b^2 - c^2 = -a'^2\delta' \frac{h_3 \cos 2\Theta_* - h_1 \sin 2\Theta_*}{h_3 \sin^2 \vartheta}\,, \tag{A4}$$

where

$$h_1 = \sin^2 \varphi - \cos^2 \varphi \cos^2 \vartheta\,, \qquad h_2 = \cos^2 \varphi - \sin^2 \varphi \cos^2 \vartheta\,, \qquad h_3 = 2 \sin \varphi \cos \varphi \cos \vartheta\,. \tag{A5}$$

Furthermore, by combination of equations (3.37), (3.38), and (3.49), we obtain

$$a'^2 + b'^2 = 2c^2 + (a^2 - c^2)(\sin^2 \varphi + \cos^2 \varphi \cos^2 \vartheta) + (b^2 - c^2)(\cos^2 \varphi + \sin^2 \varphi \cos^2 \vartheta)\,. \tag{A6}$$

If we now substitute relations (A4) in equation (A6), and use the fact that $a^2 = c^2 + (a^2 - c^2)$, then we find

$$a^2 = a'^2\left[1 - \delta' \cos \Theta_*\left(\cos \Theta_* + \frac{\cos \varphi}{\sin \varphi \cos \vartheta} \sin \Theta_*\right)\right]. \tag{A7}$$

Division of relations (A4) by this last expression then gives

$$\delta_1 = -\frac{(h_3 \cos 2\Theta_* - h_1 \sin 2\Theta_*)\delta'}{h_3 \sin^2 \vartheta\{1 - \delta' \cos \Theta_*[\cos \Theta_* + (\cot \varphi \sin \Theta_*/\cos \vartheta)]\}}\,,$$

$$\delta_2 = -\frac{(h_3 \cos 2\Theta_* + h_2 \sin 2\Theta_*)\delta'}{h_3 \sin^2 \vartheta\{1 - \delta' \cos \Theta_*[\cos \Theta_* + (\cot \varphi \sin \Theta_*/\cos \vartheta)]\}}\,. \tag{A8}$$

These are the desired expressions. Although derived for the perfect ellipsoid (3.43), the above results are independent of the density profile and hence are valid for all ellipsoids of the form (A1).

APPENDIX B

A FAMILY OF TRIAXIAL MODELS

The density distribution of the triaxial Stäckel model defined by the function $G(\tau)$ of equation (5.15) is given by Kuzmin's formula (5.12), with $\Psi(\tau)$ defined in equation (5.14) and $\psi(\tau) = \Psi'(\tau)$. First we give the explicit expressions for $\Psi(\tau)$ and $\psi(\tau)$, and then we briefly discuss some properties of the models.

I. THE FUNCTIONS $\Psi(\tau)$ AND $\psi(\tau)$

By means of equation (5.14) we find

$$\frac{4\pi G\Psi(\tau)}{A^2} = (\tau+\gamma)\left[\frac{2(\tau+\gamma)}{(\tau+\beta)(\tau+\beta+\tau_0)^p} - \frac{\gamma-\beta}{(\tau+\beta)\tau_0^p} - \frac{\gamma-\alpha}{(\beta-\alpha)(\tau+\alpha)}h(-\alpha) + \frac{(\tau+\beta)^2+(\beta-\alpha)(\gamma-\beta)}{(\tau+\alpha)(\tau+\beta)^2}h(\tau)\right], \quad \text{(B1)}$$

where we have introduced an auxiliary function $h(\tau)$, given by

$$h(\tau) = \begin{cases} \ln\left(\dfrac{\tau+\beta+\tau_0}{\tau_0}\right), & p = 1, \\ -\dfrac{1}{(p-1)}\left[\dfrac{1}{(\tau+\beta+\tau_0)^{p-1}} - \dfrac{1}{\tau_0^{p-1}}\right], & p \neq 1. \end{cases} \quad \text{(B2)}$$

The values of $\Psi(\tau)$ at $\tau = -\alpha$ and $\tau = -\beta$, where expression (B1) appears to be singular, can be calculated easily. We obtain

$$\frac{4\pi G\Psi(-\alpha)}{A^2} = \left(\frac{\gamma-\alpha}{\beta-\alpha}\right)\left\{\frac{3(\gamma-\alpha)}{(\beta-\alpha+\tau_0)^p} - \frac{\gamma-\beta}{\tau_0^p} - \frac{2(\gamma-\beta)}{\beta-\alpha}h(-\alpha)\right\},$$

$$\frac{4\pi G\Psi(-\beta)}{A^2} = (\gamma-\beta)\left\{\frac{2}{\tau_0^p} - \frac{3p(\gamma-\beta)}{2\tau_0^{p+1}} - \frac{\gamma-\beta}{(\beta-\alpha)\tau_0^p} + \frac{\gamma-\alpha}{(\beta-\alpha)^2}h(-\alpha)\right\}. \quad \text{(B3)}$$

In order to find $\psi(\tau)$, we differentiate equation (B1). This gives

$$\begin{aligned}\frac{4\pi G\psi(\tau)}{A^2} = {} & \frac{(\gamma-\beta)^2}{\tau_0^p(\tau+\beta)^2} - \frac{2p(\tau+\gamma)^2}{(\tau+\beta)(\tau+\beta+\tau_0)^{p+1}} + \frac{(\gamma-\alpha)^2}{(\beta-\alpha)(\tau+\alpha)^2}h(-\alpha) \\ & + \frac{(\tau+\gamma)[2(\tau+\alpha)(\tau+\beta)+(\tau+\beta)(\tau+\gamma)-3(\gamma-\beta)(\tau+\alpha)]}{(\tau+\alpha)(\tau+\beta)^2(\tau+\beta+\tau_0)^p} \\ & - \frac{(\gamma-\alpha)(\tau+\beta)^2(\tau+\gamma)-(\gamma-\beta)^2(\tau+\alpha)^2+(\beta-\alpha)(\gamma-\beta)(\tau+\alpha)(\tau+\gamma)}{(\tau+\alpha)^2(\tau+\beta)^3}h(\tau).\end{aligned} \quad \text{(B4)}$$

Special values are

$$\frac{4\pi G\psi(-\alpha)}{A^2} = \frac{(\gamma-\beta)^2}{(\beta-\alpha)^2\tau_0^p} + \frac{(\gamma-\alpha)(7\beta-3\alpha-4\gamma)}{(\beta-\alpha)^2(\beta-\alpha+\tau_0)^p} - \frac{5p(\gamma-\alpha)^2}{2(\beta-\alpha)(\beta-\alpha+\tau_0)^{p+1}} + \frac{(\gamma-\beta)(3\gamma-2\beta-\alpha)}{(\beta-\alpha)^3}h(-\alpha),$$

$$\frac{4\pi G\psi(-\beta)}{A^2} = \frac{2}{\tau_0^p} - \frac{2(\gamma-\beta)}{(\beta-\alpha)\tau_0^p} - \frac{(\gamma-\beta)^2}{(\beta-\alpha)^2\tau_0^p} - \frac{4p(\gamma-\beta)}{\tau_0^{p+1}} + \frac{p(\gamma-\alpha)(\gamma-\beta)}{2(\beta-\alpha)\tau_0^{p+1}} + \frac{5p(p+1)(\gamma-\beta)^2}{6\tau_0^{p+2}} + \frac{(\gamma-\alpha)^2}{(\beta-\alpha)^3}h(-\alpha),$$

$$\frac{4\pi G\psi(-\gamma)}{A^2} = \frac{1}{\tau_0^p} - \frac{h(-\gamma)}{(\gamma-\beta)} + \frac{h(-\alpha)}{(\beta-\alpha)}. \quad \text{(B5)}$$

II. MASS MODELS

The ellipsoidal coordinates (λ, μ, ν) are fixed by specification of $\gamma - \beta$ and $\gamma - \alpha$. Since τ_0 is essentially a scale length, and A is an overall scale factor, it follows that the function $\psi(\tau)$ defines a three-parameter family of Stäckel models by means of equation (5.12). The parameters are p and the rescaled semifocal distances Δ_{1*} and Δ_{2*}, given by

$$\Delta_{1*}^2 = \frac{\gamma-\beta}{\tau_0}, \qquad \Delta_{2*}^2 = \frac{\gamma-\alpha}{\tau_0}. \quad \text{(B6)}$$

For $h(\tau)$ to be well defined, we must have $\tau_0 > \gamma - \beta$, so that Δ_{1*} and Δ_{2*} must be chosen in the intervals

$$0 \leq \Delta_{1*}^2 < 1, \qquad 0 \leq \Delta_{2*}^2 < \frac{\gamma-\alpha}{\gamma-\beta}. \quad \text{(B7)}$$

We now show that p determines the radial falloff of the density at large distances from the center, and that Δ_{1*} and Δ_{2*} are related to the central axis ratios of the model defined by $\psi(\tau)$.

At large values of τ we have, for $1 \leq p < \frac{3}{2}$,

$$\frac{4\pi G\psi(\tau)}{A^2} \sim \frac{3-2p}{\tau^p} \qquad (\tau \gg 1). \quad \text{(B8)}$$

Since this profile falls off slower than $1/\tau^2$, the density distribution becomes more nearly spherical at large radii, and has infinite total mass (ZPF).

The central axis ratios of the density distribution follow from equation (35) of ZPF. We find

$$\left(\frac{a_3}{a_1}\right)^2 = \Delta_{1*}^2\left[\frac{3}{\Delta_*^2(1+\Delta_*^2)^p} - \frac{1}{\Delta_*^2} - \frac{1}{\Delta_*^2+\Delta_{1*}^2}\,k(-\Delta_{1*}^2) - \frac{\Delta_*^2+2\Delta_{1*}^2}{\Delta_*^2(\Delta_*^2+\Delta_{1*}^2)}\,k(\Delta_*^2)\right]$$
$$\times\left[1 - \frac{3}{(1-\Delta_{1*}^2)^p} + \frac{\Delta_{1*}^2}{\Delta_*^2+\Delta_{1*}^2}\,k(\Delta_*^2) + \frac{2\Delta_*^2+\Delta_{1*}^2}{\Delta_*^2+\Delta_{1*}^2}\,k(-\Delta_{1*}^2)\right]^{-1}, \tag{B9}$$

and

$$\left(\frac{a_3}{a_2}\right)^2 = \left[1 - \frac{\Delta_{1*}^2}{\Delta_*^2} - \frac{3p}{2}\,\Delta_{1*}^2 - k(-\Delta_{1*}^2) + \frac{\Delta_{1*}^2}{\Delta_*^2}\,k(\Delta_*^2)\right]\left[1 - \frac{3}{(1-\Delta_{1*}^2)^p} + \frac{\Delta_{1*}^2}{\Delta_*^2+\Delta_{1*}^2}\,k(\Delta_*^2) + \frac{2\Delta_*^2+\Delta_{1*}^2}{\Delta_*^2+\Delta_{1*}^2}\,k(-\Delta_{1*}^2)\right]^{-1}, \tag{B10}$$

where we have written $\Delta_*^2 = \Delta_{2*}^2 - \Delta_{1*}^2$. The auxiliary function $k(s)$ is defined as

$$k(s) = \begin{cases} \dfrac{1}{s}\ln(1+s)\,, & p = 1\,, \\ -\dfrac{1}{(p-1)s}\left[\dfrac{1}{(1+s)^{p-1}} - 1\right], & p \neq 1\,. \end{cases} \tag{B11}$$

For $p = 1$ the function $\psi(\tau)$ is nonnegative for all values of Δ_{1*} and Δ_{2*} allowed by equation (B7). According to Kuzmin's theorem, the associated density $\rho(\lambda, \mu, \nu)$ is nonnegative everywhere. Furthermore, $\psi(\tau)$ and $|\psi^*(\tau)|$ are monotonically decreasing functions of τ. As a result, the density distribution is triaxial, with the z-axis as short axis and the long axis in the x-direction. The surfaces of constant density are approximately ellipsoidal, with axis ratios that increase monotonically outward. The central axis ratios may become arbitrarily small. For $1 < p < \frac{3}{2}$, the function $\psi(\tau)$ is nonnegative for all $\tau \geq -\gamma$ for a large range of values of Δ_{1*} and Δ_{2*} that satisfy condition (B7). The associated models are again triaxial, with ellipticity profiles that are not monotonic and surfaces of constant density that show a larger variety in shape.

III. AXISYMMETRIC LIMITS

The expressions given above simplify considerably in the axisymmetric limiting cases. The limit $\gamma - \beta$ has been discussed in detail by de Zeeuw and Lynden-Bell (1988). In this case the mass models are prolate. In the limit $\beta = \alpha$, the ellipsoidal coordinates reduce to prolate spheroidal coordinates (λ, φ, ν), with λ and ν elliptic coordinates in a meridional plane of constant φ. The density is now given by

$$\rho(\lambda, \nu) = \frac{(\lambda+\alpha)^2}{(\lambda-\nu)^2}\,\psi(\lambda) - \frac{2(\lambda+\alpha)(\nu+\alpha)}{(\lambda-\nu)^3}\,[\Psi(\lambda) - \Psi(\nu)] + \frac{(\nu+\alpha)^2}{(\nu-\lambda)^2}\,\psi(\nu)\,, \tag{B12}$$

with

$$\frac{4\pi G\Psi(\tau)}{A^2} = \left(\frac{\tau+\gamma}{\tau+\alpha}\right)\left[\frac{2(\tau+\gamma)}{(\tau+\alpha+\tau_0)^p} - \frac{2(\gamma-\alpha)}{\tau_0^p} + h(\tau)\right], \tag{B13}$$

and

$$\frac{4\pi G\psi(\tau)}{A^2} = -\frac{2p(\tau+\gamma)^2}{(\tau+\alpha)(\tau+\alpha+\tau_0)^{p+1}} + \frac{2(\gamma-\alpha)^2}{(\tau+\alpha)^2\tau_0^p} + \frac{(\tau+\gamma)(3\tau+5\alpha-2\gamma)}{(\tau+\alpha)^2(\tau+\alpha+\tau_0)^p} - \frac{(\gamma-\alpha)}{(\tau+\alpha)^2}\,h(\tau)\,, \tag{B14}$$

where $h(\tau)$ was defined in equation (B2), and we take $\beta = \alpha$. For $p = 1$ these expressions can be simplified further (cf. Statler 1988):

$$\frac{4\pi G\Psi(\tau)}{A^2} = (\tau+\gamma)\left[\frac{2(\tau_0+\alpha-\gamma)}{\tau_0(\tau+\alpha+\tau_0)} + \frac{1}{\tau+\alpha}\ln\left(\frac{\tau+\alpha+\tau_0}{\tau_0}\right)\right],$$
$$\frac{4\pi G\psi(\tau)}{A^2} = \frac{2(\tau_0+\alpha-\gamma)^2}{\tau_0(\tau+\alpha+\tau_0)^2} + \frac{\tau+\gamma}{(\tau+\alpha)(\tau+\alpha+\tau_0)} - \frac{\gamma-\alpha}{(\tau+\alpha)^2}\ln\left(\frac{\tau+\alpha+\tau_0}{\tau_0}\right). \tag{B15}$$

Useful special values are

$$\frac{4\pi G\Psi(-\alpha)}{A^2} = (\gamma-\alpha)\left\{\frac{1}{\tau_0^p} + \frac{2[\tau_0 - p(\gamma-\alpha)]}{\tau_0^{p+1}}\right\},$$
$$\frac{4\pi G\psi(-\alpha)}{A^2} = \frac{3}{\tau_0^p} - \frac{9p(\gamma-\alpha)}{2\tau_0^{p+1}} + \frac{p(p+1)(\gamma-\alpha)^2}{\tau_0^{p+2}},$$
$$\frac{4\pi G\psi(-\gamma)}{A^2} = \frac{2}{\tau_0^p} - \frac{h(-\gamma)}{\gamma-\alpha}. \tag{B16}$$

The behavior of $\psi(\tau)$ as $\tau \to \infty$ is the same as given in equation (B8).

Equation (B12) describes a two-parameter family of oblate mass models. As in the triaxial case, the parameter p determines the slope of the density profile at large radii. The parameter $\Delta_{1*} = \Delta_{2*} = (\gamma - \alpha)/\tau_0$, which according to equation (B7) must satisfy $0 \leq \Delta_{1*}^2 < 1$, is related to the central axis ratio of the mass model, which is given by

$$\left(\frac{a_3}{a_1}\right)^2 = \frac{1 - 2p\Delta_{1*}^2 - k(-\Delta_{1*}^2)}{2 - 3/(1 - \Delta_{1*}^2)^p + k(-\Delta_{1*}^2)} . \tag{B17}$$

For $\Delta_{1*}^2 \sim 0$, i.e., for nearly spherical models, we find

$$\left(\frac{a_3}{a_1}\right)^2 \sim 1 - \frac{7(p+1)}{15}\Delta_{1*}^2 \qquad (\Delta_{1*}^2 \ll 1) . \tag{B18}$$

REFERENCES

Bertola, F. 1987, in *IAU Symposium 127, Structure and Dynamics of Elliptical Galaxies*, ed. P. T. de Zeeuw (Dordrecht: Reidel), p. 135.
Bertola, F., Bettoni, D., Danziger, J., Sadler, E. M., Sparke, L. S., and de Zeeuw, P. T. 1989*a*, in preparation.
Bertola, F., Rubin, V., and Zeilinger, W. W. 1989*b*, *Ap. J.* (*Letters*), submitted.
Binney, J. J. 1978, *Comments Ap.*, **8**, 27.
———. 1985, *M.N.R.A.S.*, **212**, 769.
Binney, J. J., and de Vaucouleurs, G. 1981, *M.N.R.A.S.*, **194**, 679.
Bland, J., Taylor, K., and Atherton, P. D. 1987, *M.N.R.A.S.*, **228**, 595.
Burbidge, E. M., Burbidge, G. R., and Prendergast, K. H. 1959, *Ap. J.*, **130**, 739.
Contopoulos, G. 1956, *Zs. Ap.*, **39**, 126.
Davies, R. L. 1987, in *IAU Symposium 127, Structure and Dynamics of Elliptical Galaxies*, ed. P. T. de Zeeuw (Dordrecht: Reidel), p. 63.
de Zeeuw, P. T. 1985*a*, *M.N.R.A.S.*, **216**, 273 (Z85).
———. 1985*b*, *M.N.R.A.S.*, **216**, 599.
de Zeeuw, P. T., and Lynden-Bell, D. 1985, *M.N.R.A.S.*, **215**, 713.
———. 1988, *M.N.R.A.S.*, **232**, 419.
de Zeeuw, P. T., Peletier, R. F., and Franx, M. 1986, *M.N.R.A.S.*, **221**, 1001 (ZPF).
de Zeeuw, P. T., and Pfenniger, D. 1988, *M.N.R.A.S.*, **235**, 949.
Ebneter, K., and Balick, B. 1985, *A.J.*, **90**, 183.
Franx, M. 1988, *M.N.R.A.S.*, **231**, 285.
Gerhard, O. E. 1985, *Astr. Ap.*, **151**, 279.
Gerhard, O. E., and Vietri, M. 1986, *M.N.R.A.S.*, **223**, 377.
Gerhard, O. E., Vietri, M., and Kent, S. 1989, *Ap. J.* (*Letters*), submitted.
———. 1987, in *IAU Symposium 127, Structure and Dynamics of Elliptical Galaxies*, ed. P. T. de Zeeuw (Dordrecht: Reidel), p. 401.
Gunn, J. E. 1979, in *Active Galactic Nuclei*, ed. C. Hazard and S. Mitton (Cambridge: Cambridge University Press), p. 213.
Habe, A., and Ikeuchi, S. 1985, *Ap. J.*, **289**, 540.
———. 1988, *Ap. J.*, **326**, 84.
Hawarden, T. G., Elson, R. A. W., Longmore, A. J., Tritton, S. B., and Corwin, H. G. 1981, *M.N.R.A.S.*, **196**, 747.
Heiligman, G., and Schwarzschild, M. 1979, *Ap. J.*, **233**, 872.
Heisler, J., Merritt, D. R., and Schwarzschild, M. 1982, *Ap. J.*, **258**, 490.
Kondrat'ev, B. P., and Ozernoy, L. M. 1979, *Soviet. Astr. Letters*, **5**, 37.
Kuzmin, G. G. 1973, in *Proc. All-Union Conf. on Dynamics of Galaxies and Clusters*, ed. T. B. Omarov (Alma Ata: Akademiya Nauk Kazakhskoj SSR), p. 71. English transl. in *IAU Symposium 127, Structure and Dynamics of Elliptical Galaxies*, ed. P. T. de Zeeuw [Dordrecht: Reidel, 1987], p. 553).
Kuzmin, G. G., and Kutuzov, S. A. 1966, *Pub. Tartu Ap. Obs.*, **35**, 316.
Magnenat, P. 1982, *Astr. Ap.*, **108**, 95.
Merritt, D. R., and de Zeeuw, P. T. 1983, *Ap. J.* (*Letters*), **267**, L23.
Rybicki, G. B. 1987, in *IAU Symposium 127, Structure and Dynamics of Elliptical Galaxies*, ed. P. T. de Zeeuw (Dordrecht: Reidel), p. 397.
Schechter, P. L. 1987, in *IAU Symposium 127, Structure and Dynamics of Elliptical Galaxies*, ed. P. T. de Zeeuw (Dordrecht: Reidel), p. 217.
Schwarzschild, M. 1979, *Ap. J.*, **232**, 236.
Schweizer, F., Whitmore, B. C., and Rubin, V. C. 1983, *A.J.*, **88**, 909.
Sparke, L. S. 1986, *M.N.R.A.S.*, **219**, 657.
Stark, A. A. 1977, *Ap. J.*, **213**, 368.
Statler, T. S. 1988, *Ap. J.*, **331**, 71.
Steiman-Cameron, T. Y., and Durisen, R. H. 1982, *Ap. J.* (*Letters*), **263**, L63.
———. 1988, *Ap. J.*, **325**, 26.
Teuben, P. J. 1987, *M.N.R.A.S.*, **227**, 815.
Tohline, J. E., Simonson, G. F., and Caldwell, N. 1982, *Ap. J.*, **252**, 92.
Tremaine, S. D., and Weinberg, M. D. 1985, *Ap. J.* (*Letters*), **282**, L5.
Tubbs, A. D. 1980, *Ap. J.*, **241**, 969.
van Albada, T. S., Kotanyi, C. G., and Schwarzschild, M. 1982, *M.N.R.A.S.*, **198**, 303.
van Albada, T. S., and Sancisi, R. 1986, *Phil. Trans. Roy. Soc. London, A*, **320**, 447.
van Albada, T. S., and Sanders, R. H. 1982, *M.N.R.A.S.*, **201**, 303.
Varnas, S. R. 1986, *Proc. Astr. Soc. Australia*, **6**, 458.
Whitmore, B. C., Schweizer, F., and McElroy, D. B. 1987*a*, *Ap. J.*, **314**, 439.
———. 1987*b*, in *IAU Symposium 127, Structure and Dynamics of Elliptical Galaxies*, ed. P. T. de Zeeuw (Dordrecht: Reidel), p. 413.
Wilkinson, A., Sharples, R. M., Fosbury, R. A. E., and Wallace, P. T. 1986, *M.N.R.A.S.*, **218**, 297.

P. T. De Zeeuw: Theoretical Astrophysics, 130-33, California Institute of Technology, Pasadena, CA 91125

M. Franx: Harvard-Smithsonian Center for Astrophysics, Cambridge, MA 02138